



PCCP

Double Rydberg Anions, Rydberg Radicals and Micro-solvated Cations with Ammonium-Water Kernels

Journal:	<i>Physical Chemistry Chemical Physics</i>
Manuscript ID	CP-ART-06-2022-002570.R1
Article Type:	Paper
Date Submitted by the Author:	13-Jul-2022
Complete List of Authors:	Opoku, Ernest; Auburn University, Chemistry and Biochemistry Pawlowski, Filip; Auburn University, Chemistry and Biochemistry Ortiz, Joseph; Auburn University, Department of Chemistry and Biochemistry

SCHOLARONE™
Manuscripts

Double Rydberg Anions, Rydberg Radicals and Micro-solvated Cations with Ammonium-Water Kernels

Ernest Opoku, Filip Pawłowski and Joseph Vincent Ortiz*

Department of Chemistry and Biochemistry, Auburn University,
Auburn, AL 36849-5312, United States

ezo0009@auburn.edu, filip@auburn.edu, ortiz@auburn.edu

13 July 2022

Abstract

Highly accurate *ab initio* electron-propagator and coupled-cluster methods are employed to predict the vertical electron attachment energies (VEAEs) of $\text{NH}_4^+(\text{H}_2\text{O})_n$ ($n=1-4$) cationic clusters. The VEAEs decrease with increasing n and the corresponding Dyson orbitals are diffused over peripheral, non-hydrogen bonded protons. Clusters formed from NH_4^- double Rydberg anions (DRAs) and stabilized by hydrogen bonding or electrostatic interactions are studied through calculations on $\text{NH}_4^-(\text{H}_2\text{O})_n$ complexes and are compared with more stable $\text{H}^-(\text{NH}_3)(\text{H}_2\text{O})_n$ isomers. Structures that have cationic and anionic congeners have notable changes in geometry. For all values of n , the hydride-molecule complex $\text{H}^-(\text{NH}_3)(\text{H}_2\text{O})_n$ is always the most stable, with large vertical electron detachment energies (VEDEs). $\text{NH}_4^-(\text{H}_2\text{O})_n$ DRA isomers are predicted to have VEDEs that correspond to energetically well-separated peaks in an anion photoelectron spectrum. Less stable DRA isomers display proton donation from the tetrahedral NH_4^- fragment to water molecules and VEDEs close to those of previously discovered DRAs. The most stable DRA isomers feature tetrahedral NH_4^- fragments without H bridges to water molecules and VEDEs that increase with n . Dyson orbitals of $\text{NH}_4^-(\text{H}_2\text{O})_n$ DRAs occupy regions beyond the exterior non-bridging O-H and N-H bonds. Thus, the Rydberg electrons in the uncharged Rydberg radicals and DRAs are held near the outer protons of the water and ammonia molecules. Several bound low-lying excited states of the doublet Rydberg radicals have single electrons occupying delocalized Dyson orbitals of *s*-like, *p*-like, *d*-like, or *f*-like nodal patterns with the following Aufbau principle: 1s, 1p, 1d, 2s, 2p, 1f.

Keywords: Double Rydberg Anions; Rydberg Radicals; Electron Propagator Theory; Dyson Orbitals; Molecular Spectra; Solvated Electron Precursors

1. INTRODUCTION

In double Rydberg anions (DRAs), a closed-shell, cationic core binds a pair of electrons held in diffuse orbitals. For example, in the NH_4^- or OH_3^- DRAs, an ammonium or hydronium cation is surrounded by a pair of peripheral electrons. The first DRA, tetrahedral NH_4^- , was discovered by Bowen and co-workers^{1,2} during a pioneering photoelectron spectroscopic study on an anion-molecule complex, $\text{H}^-(\text{NH}_3)$. As the NH_4^- DRA and $\text{H}^-(\text{NH}_3)$ have identical mass, their electron detachment energies appeared as separate peaks in the same spectrum. The persistence of the spectral peak at a low vertical electron detachment energy (VEDE) under a variety of ion-source conditions, the absence of an energetic shift after full deuterium substitution for the hydrogens and previous investigations on the NH_4 radical³ led to the identification of tetrahedral NH_4^- as a DRA. The measured^{1,2} VEDE of NH_4^- was 0.472 eV, an amount resembled that of the sodium atomic anion (0.548 eV).⁴

High-level theoretical calculations have provided strong complementary support for the identification of DRAs. Prior to the discovery¹ of the NH_4^- DRA, some theoretical studies^{5,6} had considered the existence of a tetrahedral isomer of NH_4^- . Ortiz applied techniques of *ab initio* electron propagator theory (EPT) to study the geometric isomers and vertical ionization energies of NH_4^- and proposed the tetrahedral structure to be a viable DRA.⁷ The two stable isomers were assigned to a hydride-molecule complex $\text{H}^-(\text{NH}_3)$ and a tetrahedral counterpart, NH_4^- , with VEDEs of 1.20 eV and 0.42 eV, respectively, in precise agreement with the experimental^{1,2} results. Evidence of the diffuse, Rydberg-state distribution of the two diffuse electrons which surround the NH_4^+ cationic core was provided.⁷ Subsequent theoretical studies⁸⁻¹² on the NH_4^- DRA also reported the VEDE to be near 0.45 eV.

Photoelectron spectroscopy has enabled the identification of several DRA clusters among the $\text{N}_n\text{H}_{3n+1}^-$ ($n=1-5$) isomers.^{13,14} Isomers of DRAs belong to three categories: (1) hydrides coordinated to n solvent molecules, (2) electrostatically bound intermolecular complexes with solvent molecules and (3) hydrogen-bonded DRA-molecule complexes. *Ab initio* EPT studies^{15,16} have revealed identical isomeric patterns and electron binding energies in close agreement with experimental data. More recent EPT investigations¹⁷ have found three new classes of DRAs: methylated, annulated, and paramagnetic. Prior to this investigation, Hopper *et al.*¹⁸ reported the existence of NH_3R^- and OH_2R^- ($\text{R} = \text{F}, \text{OH}, \text{NH}_2, \text{and } \text{CH}_3$) sets of DRAs that are stable minima in their potential energy surfaces and have positive VEDEs. A tetrahedral PH_4^- DRA has been identified in a study that also predicted a C_{2v} isomer with a lone-pair of electrons occupying an equatorial position in a trigonal bipyramidal arrangement.¹²

Ortiz¹⁹ performed computational studies on OH_3^- isomers and identified a pyramidal, C_{3v} DRA with a VEDE of 0.43 eV. However, several experimental efforts to characterize the OH_3^- DRA have not been successful. Melin and Ortiz²⁰ therefore conducted *ab initio* EPT studies on the reaction barrier between the OH_3^- DRA and a hydride-water complex. The barrier between the NH_4^- DRA and a hydride-ammonia complex also was examined. The low reaction barrier between the OH_3^- DRA and the hydride-water complex indicates that the former species may be difficult to isolate. Evidence of the existence of O_2H_5^- DRAs in analogy with N_2H_7^- was also reported.²⁰ Several DRAs based on elements other than N are also known from computational studies.²¹

DRA, Rydberg radicals, their electronic structure and reactivity have been reviewed elsewhere.^{10,22} The lowest diffuse orbitals in DRAs and Rydberg radicals are spheroidal and mimic valence s orbitals of alkali atoms. In their excited states, orbitals with major contributions from diffuse s-, p-, d-, f-, or g functions may be occupied. Large molecular systems (such as clusters) may feature different types of Rydberg states and orbitals.^{23,24} Previous²⁵ and recent²⁶ studies have established that these unique molecular systems also participate in Rydberg-type chemical bonding in analogy with alkali-metal diatomic molecules and larger clusters.²⁷ Rydberg patterns of chemical bonding also manifest in protein fragments.^{28,29}

Discovery and identification of novel DRAs and solvated-electron precursors^{30–32} (which include metal-ammonia complexes with diffuse electrons) have relied heavily on techniques of *ab initio* EPT.^{7,20} In a recent publication³³ on this subject, we extended the scope of the DRA concept to oxygen-based systems with the general formula $O_nH_{2n+1}^-$. Isomers that feature hydride-water interactions were compared with species in which the pyramidal H_3O^- DRA is stabilized by ion-dipole or hydrogen-bonding interactions with water molecules. For all values of n studied, the anion-water complex $H^-(H_2O)_{n+1}$ is always the most stable and has relatively large VEDEs. DRA-molecule complexes (i.e., $OH_3^-(H_2O)_n$ isomers) have much lower VEDEs and may be detectable in anion photoelectron spectra. For all $O_nH_{2n+1}^-$ DRAs, Dyson orbitals occupy regions beyond the peripheral O-H bonds. We also calculated the vertical electron attachment energies (VEAEs) of $OH_3^+(H_2O)_n$ clusters and excitation energies of the $OH_3^+(H_2O)_n$ Rydberg radicals. The VEAEs decrease with increasing n and the corresponding Dyson orbitals are diffused over exterior, non-hydrogen bonded protons.

Can the concepts of DRAs and their ion-molecule clusters be extended to systems in which the cationic kernel is not a protonated micro-solvent molecule? Are the same extensions applicable to Rydberg radicals and their micro-solvated clusters? These questions prompted a thorough search of the chemical literature and evidence of ammonium-water cationic clusters $NH_4^+(H_2O)_n$ ³⁴ was found. Structural and energetic properties of $NH_4^+(H_2O)_n$ clusters were probed³⁵ by free jet expansion experiments and *ab initio* calculations decades ago. Later computational studies also found several other low-lying isomers.^{36–39} At the MP2 level of theory, in conjunction with correlated basis sets, Morrell and Shields⁴⁰ studied the $NH_4^+(H_2O)_n$ ($n=1–10$) isomers with a view to their atmospheric abundance as a function of temperature. Pei *et. al.*³⁴ also presented an extensive study on $NH_4^+(H_2O)_n$ ($n=1–10$) isomers and the effects of temperature and humidity on cluster growth patterns.

$NH_4^+(H_2O)_n$ clusters are reportedly abundant in the biosphere and an understanding of them is essential for modeling atmospheric and interstellar processes.⁴¹ Studies on electronic structure and properties of molecular ions in aqueous media provide theoretical guidance in many chemical and biological processes.^{42–44} Concepts of acid-base chemistry, redox reactions, electrochemistry, and a multitude of organic and inorganic reactions are often defined in terms of proton and electron transfer. Understanding the behavior of protons and electrons in aqueous media is a perennial concern in physical chemistry.

Structure and bonding in micro-solvated $NH_4^{+,0,-}(H_2O)_n$ ($n=1–4$) clusters therefore deserve further study. All cationic $NH_4^+(H_2O)_n$ isomers reported in the literature so far are reconsidered. Addition of an electron produces uncharged clusters in which an NH_4 Rydberg radical is coordinated to water molecules. Excitation energies of several low-lying states of $NH_4(H_2O)_n$ Rydberg radicals are also

calculated. Three kinds of anionic structures emerge from geometry optimizations. Micro-solvated hydride anions are denoted henceforth by $\text{H}^-(\text{NH}_3)(\text{H}_2\text{O})_n$. The NH_4^- DRA with coordinated water molecules is represented by $[\text{NH}_4^-](\text{H}_2\text{O})_n$. The formula $\text{NH}_4^-(\text{H}_2\text{O})_n$ stands for structures with two diffuse electrons and a cationic kernel in which ammonium forms hydrogen bonds with water molecules.

We have employed correlated *ab initio* electron-propagator and coupled-cluster methods with large, diffuse basis sets to study $\text{NH}_4^+(\text{H}_2\text{O})_n$ clusters, $\text{NH}_4(\text{H}_2\text{O})_n$ Rydberg molecules, $\text{H}^-(\text{NH}_3)(\text{H}_2\text{O})_n$, $[\text{NH}_4^-](\text{H}_2\text{O})_n$, $\text{NH}_4^-(\text{H}_2\text{O})_n$ DRAs and related micro-solvated species. The primary focus of this work is prediction of structures, relative total energies, vertical electron binding energies and Dyson orbitals of $\text{NH}_4^{+,0,-}(\text{H}_2\text{O})_n$ ($n=1-4$) clusters. Calculations on micro-solvated $\text{NH}_4^{+,0,-}(\text{H}_2\text{O})_n$ ($n=1-4$) clusters provide Aufbau rules for electrons that occupy the periphery of these complexes.

2. THEORY AND COMPUTATIONAL DETAILS

2.1 Summary of electron propagator theory

Ab initio methods of EPT⁴⁵⁻⁴⁷ calculate electron binding energies directly, i.e., without any explicit reference to final state wave functions and their total energies. Electron attachment and detachment energies occur at poles of the electron propagator matrix, $\mathbf{G}(E)$, whose elements read

$$G_{rs}(E) = \lim_{\eta \rightarrow +0} \left[\sum_P^{\text{Attachment}} \frac{\langle 0 | a_r | P \rangle \langle P | a_s^\dagger | 0 \rangle}{E + E_0 - E_P^+ + i\eta} + \sum_P^{\text{Detachment}} \frac{\langle 0 | a_s^\dagger | P \rangle \langle P | a_r | 0 \rangle}{E - E_0 + E_P^- - i\eta} \right], \quad (1)$$

where the N -electron reference state, $|0\rangle$, and the $(N\pm 1)$ -electron final states, $|P\rangle$, and their energies (E_0 and E_P^\pm , respectively) are the solutions to the Hamiltonian eigenvalue problem,

$$\begin{aligned} H |0\rangle_N &= E_0 |0\rangle_N, \\ H |P\rangle_{N\pm 1} &= E_P^\pm |P\rangle_{N\pm 1}, \end{aligned} \quad (2)$$

a_r and a_s^\dagger are annihilation and creation operators, respectively, with spin-orbital indices, r and s , and the infinitesimal factor η ensures the correct Fourier transformation between the time-dependent definition of the electron propagator and its energy representation. Electron binding energies occur at the poles (i.e., vanishing denominators) of Equation 1. The residues (numerators) are products of Feynman-Dyson amplitudes,

$$C_{rP} = \begin{cases} \langle 0 | a_r | P \rangle, & \text{(electron attachment)} \\ \langle P | a_r | 0 \rangle, & \text{(electron detachment)} \end{cases}, \quad (3)$$

and their complex conjugates, which suffice to construct Dyson spin-orbitals (ϕ^{Dyson}) of attachment and detachment. Thus, changes in electronic structure between the initial state, $|0\rangle$, and the $(N\pm 1)$ -electron final states, $|P\rangle$, are represented by Dyson orbitals of electron detachment,

$$\phi_P^{\text{Dyson}}(x_1) = N^{1/2} \int dx_2 dx_3 \cdots dx_N \Psi_{N,0}(x_1, x_2, x_3, \cdots, x_N) \Psi_{N-1,P}^*(x_2, x_3, \cdots, x_N), \quad (4)$$

or those of electron attachment,

$$\phi_P^{\text{Dyson}}(x_1) = (N+1)^{1/2} \int dx_2 dx_3 \cdots dx_{N+1} \Psi_{N+1,P}(x_1, x_2, x_3, \cdots, x_{N+1}) \Psi_{N,0}^*(x_2, x_3, \cdots, x_{N+1}). \quad (5)$$

The probability factor (also known as the intensity factor, pole strength, or the norm of the Dyson orbital), Γ_p , may be used to normalize the Dyson spin-orbitals of equations 4 and 5 such that the unit-normalized Dyson spin-orbital, ϕ^{Dyson} , reads

$$\phi_p^{\text{Dyson}} = \Gamma_p^{-0.5} \phi_p^{\text{Dyson}}. \quad (6)$$

When the canonical Hartree-Fock reference state and the Møller-Plesset partitioning of the Hamiltonian are employed, the inverse electron propagator matrix takes the form

$$\mathbf{G}^{-1}(E) = \mathbf{E}\mathbf{I} - \boldsymbol{\varepsilon} - \boldsymbol{\sigma}(E), \quad (7)$$

where $\boldsymbol{\varepsilon}$ is a diagonal matrix of Hartree-Fock orbital energies and $\boldsymbol{\sigma}(E)$ is the self-energy matrix, which describes orbital relaxation in final states and differential electron correlation between initial and final states. Poles occur at values of E that yield vanishing eigenvalues of $\mathbf{G}^{-1}(E)$. Neglect of the self-energy matrix recovers the (zeroth-order) Koopmans's theorem (KT)⁴⁸ result. (The first-order correction vanishes.) In many low-order methods, off-diagonal elements of $\boldsymbol{\sigma}(E)$ in the canonical Hartree-Fock orbital basis are neglected. Subsequent retention of all terms through second or third order in the self-energy matrix leads to the diagonal, second-order (D2),^{46,49} and diagonal third order (D3) methods.^{46,49,50} Approximate treatments of higher order self-energy terms (i.e., renormalizations that pertain to certain classes of self-energy terms in all orders of perturbation theory) that require almost no additional computational effort include the A, B and C variants of the outer-valence Green's function (OVGF).^{51–53} Numerical criteria have been introduced to automatically choose among these variants in a given calculation.^{51,53,54} An alternative, parameter-free approach to diagonal, low-order approximations which has achieved superior accuracy with lower cost has yielded the partial third-order (P3)⁵⁵ method and its approximately renormalized counterpart (P3+).^{46,49} OVGF and P3+ have been highly successful^{56–58} in describing valence detachment energies and electron affinities of systems for which KT constitutes a valid zeroth-order approximation. We have recently derived a new generation of diagonal EP methods from an intermediately normalized, Hermitized metric that retain the computational advantages of their antecedents, but with higher accuracy.⁵⁹ When the probability factor obtained with one of the aforementioned approximations is below 0.85,⁶⁰ the results should be treated with caution. This typically happens for systems with strong correlation (such as DRAs, *vide infra*) in the initial state. Such cases require employment of non-diagonal, renormalized techniques⁶¹ such as the BD-T1^{50,61–63} method.

2.2 Geometry optimizations, vibrational frequencies, vertical electron binding energies and excitation energies

For cationic geometries, initial guess inputs were obtained by constraining specific internal coordinates of the cations (bond lengths, bond angles, dihedral angles) and optimizing the remaining internal coordinates. The resulting geometries were then used as an input for full geometry optimizations without any geometry or symmetry constraints. The geometries of optimized cationic isomers are identical to those in published works^{34,36–39} on $\text{NH}_4^+(\text{H}_2\text{O})_n$ clusters. The fully optimized cationic geometries were used as initial guess input structures for full anionic geometry optimizations. Initial input structures for the remaining anionic geometries (hydride-molecule complexes, DRA-

molecule complexes) were obtained through informed guesses in analogy with nitrogen-based $N_nH_{3n+1}^-$ ¹⁶ and oxygen-based $O_nH_{2n+1}^-$ DRAs.³³

Structures of cations and anions were optimized at the MP2 level in conjunction with the augmented, correlation-consistent, triple- ζ (aug-cc-pVTZ)^{64,65} basis. The same level of theory was found to be sufficient for cations and anions in previous studies on $O_nH_{2n+1}^{+,0,-}$ clusters.^{20,33} Vibrational frequencies of all the optimized geometries were real and positive.

Single-point energy calculations at the coupled-cluster singles-and-doubles (CCSD)⁶⁶ and coupled-cluster singles-and-doubles with perturbative triples (CCSD(T))⁶⁷ levels were carried out on the MP2/aug-cc-pVTZ optimized geometries to infer relative energies. To obtain vertical electron affinities or ionization energies based on the indirect coupled-cluster methods (Δ CCSD and Δ CCSD(T)), single-point calculations on the $NH_4(H_2O)_n$ radicals were performed at the equilibrium geometry of cationic or anionic $NH_4^{+,-}(H_2O)_n$ ($n = 1-4$) complexes. Unrestricted Hartree-Fock spin contaminations from the UCCSD and UCCSD(T) single-point calculations on the doublet Rydberg radicals were minor.

VEAEs of ground-state cations, $NH_4^+(H_2O)_n$, that correspond to various final states of $NH_4(H_2O)_n$ doublet Rydberg radicals and VEDEs from the anions, $NH_4^-(H_2O)_n$, were calculated with EPT methods at the optimized geometries of selected ions. Several bound low-lying vertical excitation energies of the doublet Rydberg radicals were inferred from differences between the vertical electron affinities.

2.3 Basis sets for EPT and Coupled-Cluster Calculations

At the geometries of cations and anions, several basis sets were tested for calculation of electron binding energies to find a suitable balance between accuracy and computational cost. For selected systems, we tested the aug-cc-pVXZ ($X = T, Q$), d-aug-cc-pVTZ, t-aug-cc-pVTZ and q-aug-cc-pVTZ basis sets (the latter three basis sets contain respectively two, three and four sets of diffuse, primitive functions with exponents obtained in the even-tempered manner starting from the exponents of the diffuse set of the original aug-cc-pVTZ basis).⁶⁸ For both cations and anions, we found the d-aug-cc-pVTZ basis to be the optimal choice. The t-aug-cc-pVTZ, q-aug-cc-pVTZ, and aug-cc-pVQZ basis sets yield electron binding energies of similar quality as d-aug-cc-pVTZ. (See the performance of the tested basis sets in Tables S1-S3 of the electronic supporting information, or ESI). In indirect coupled-cluster (Δ CCSD and Δ CCSD(T)) calculations for determining electron binding energies, the d-aug-cc-pVTZ basis set was found to be sufficient. Therefore, unless stated otherwise, all the EPT, Δ CCSD and Δ CCSD(T) results discussed in the text were executed with the d-aug-cc-pVTZ basis. Identical conclusions have been reached elsewhere for $O_nH_{2n+1}^-$ DRAs.³³

2.4 Software

Full geometry optimizations, frequency analyses, coupled-cluster (CCSD and CCSD(T)), KT, D2, D3, OVG(A, B, C), P3 and P3+ EPT calculations were carried out with Gaussian 16.⁶⁹ The BD-T1 EP method has been implemented in a development version of Gaussian.⁷⁰ Dyson orbitals were plotted with GaussView⁷¹ using a cube file with an enhanced edge size generated with Molden.⁷² The Dyson orbitals were plotted with an iso-value of 0.08 a.u and 0.004 a.u for the cations and anions, respectively. The red and green surfaces of Dyson orbitals displayed in all Figures correspond to opposite phases of a real-valued wavefunction. The surfaces of the Dyson orbitals are semi-transparent (to display the underlying molecular framework) and therefore the inner, nodal surfaces are also visible.

3. RESULTS AND DISCUSSION

3.1 Isomers, Relative Energies, Electron Affinities and Dyson Orbitals of $\text{NH}_4^+(\text{H}_2\text{O})_n$ Cations

In this section, we present results for the optimized ground-state geometries of closed-shell $\text{NH}_4^+(\text{H}_2\text{O})_n$ isomers. For each given n , the isomers, relative energies, and geometric parameters are discussed and compared with previously reported results (if any). The lowest VEAEs and associated Dyson orbitals obtained with the direct *ab initio* EPT methods—KT, D2, D3, OVGf, P3, and P3+—are discussed and compared with indirect coupled-cluster results, i.e., ΔCCSD and $\Delta\text{CCSD(T)}$. Table I presents data on relative energies of all $\text{NH}_4^+(\text{H}_2\text{O})_n$ isomers and VEAEs obtained with diagonal, perturbative *ab initio* EPT methods and indirect coupled-cluster methods. Figures 1–4 also display the Dyson orbitals of electron attachment to the saturated $\text{NH}_4^+(\text{H}_2\text{O})_n$ cations. Detailed results on relative energies and VEAEs of the $\text{NH}_4^+(\text{H}_2\text{O})_n$ isomers are presented in Tables S4–S6.

The lowest VEAEs (Table I) for all $\text{NH}_4^+(\text{H}_2\text{O})_n$ isomers do not show much disparity between EPT methods. All EPT methods yield pole strengths above 0.85 and therefore lend credence to the adequacy of the diagonal, perturbative EPT methods. Hence, unless stated otherwise, discussion of the VEAEs and Dyson orbitals of the cations is based on the renormalized partial third order approximation (P3+) results.⁴⁹ VEAEs obtained with the indirect $\Delta\text{CCSD(T)}$ method and the d-aug-cc-pVTZ basis are in close agreement with those from EPT methods.

$\text{NH}_4^+(\text{H}_2\text{O})$:

Optimized $\text{NH}_4^+(\text{H}_2\text{O})$ possesses a linear chain geometry and belongs to the C_2 point group as observed in the Zundel O_2H_5^+ cation.³³ The length of the hydrogen bond between the NH_4^+ fragment and the H_2O molecule is 1.64 Å. Thus, $\text{NH}_4^+(\text{H}_2\text{O})$ forms an asymmetrically bridged $\text{NH}_4^+(\text{H}_2\text{O})$ complex that is unlike the symmetric hydrogen bond found in the Zundel O_2H_5^+ cation.³³ The $\text{NH}_4^+(\text{H}_2\text{O})$ complex resembles that of $\text{NH}_4^+(\text{NH}_3)$, which has been found as the central cationic kernel in $\text{H}^+(\text{NH}_3)_n$, $n = 18, 20, 25, 30$ clusters.⁷³ A search for an unusual isomer in which a binary-type hydrogen bond exists between two protons of the NH_4^+ fragment and the O nucleus of the H_2O molecule converged to the linear chain geometry as observed in previous studies.^{34,74,75} As the $\text{NH}_4^+(\text{H}_2\text{O})$ complex has a VEA of 3.748 eV which is lower than the ionization potentials (IPs) of all alkaline atoms, it can be identified as a superalkali.⁷⁶ The Dyson orbital is quasi-spherical, with its maximum amplitudes near the NH_4^+ fragment (Figure 1). The discernable orthogonalization to valence s functions on the oxygen and nitrogen nuclei contributes to the red contours. A similar Dyson orbital was identified in the Zundel O_2H_5^+ cation.³³

$\text{NH}_4^+(\text{H}_2\text{O})_2$ isomers:

Two isomers, **2a** and **2b**, emerge from the addition of a water molecule to the $\text{NH}_4^+(\text{H}_2\text{O})$ cation. In the triangular geometry **2a**, the lengths of the hydrogen bonds are 1.7172 and 1.7104 Å. In **2b**, the new H_2O molecule prefers to form a water dimer with the H_2O in the $\text{NH}_4^+(\text{H}_2\text{O})$ cation. The hydrogen bond in the water dimer occurs at a length of 1.6921 Å. The proton lies at a typical covalent distance of 1.0753 Å from the nitrogen nucleus and exhibits an O-H separation of 1.5379 Å that is characteristic of a hydrogen bond. Relative energies in Table I show that **2a** is more stable than **2b**. Conclusions from previous studies^{34,74,77} are in good agreement with our results and observations. The global minimum **2a** has a VEA of 3.226 eV, which is 0.522 eV lower than the value for the $\text{NH}_4^+(\text{H}_2\text{O})$ cation. Thus, superalkali⁷⁶ character increases with addition of a water molecule. An s -like Dyson orbital is obtained in both **2a** and **2b**. The Dyson orbitals (Figure 2) have their largest

amplitudes near the non-bonded proton positions of the NH_4^+ fragment in both isomers.

$\text{NH}_4^+(\text{H}_2\text{O})_3$ isomers:

Figure 3 displays the optimized geometries and Dyson orbitals of three $\text{NH}_4^+(\text{H}_2\text{O})_3$ isomers, **3a**, **3b**, and **3c**. **3a** has a rhombus C_{2v} geometry, whereas **3b** has a tapered geometry belonging to the C_3 point group. **3c** exhibits a linear chain structure. Relative energies (Table I) favor the tapered C_3 geometry, **3b**, as the global minimum in agreement with some past studies based on density functional calculations.^{34,74} The length of the H bonds between ammonium and water is 1.7702 Å in isomer **3b**. The geometry of **3a** is comparable to the lowest-energy geometry of the pure water cluster $(\text{H}_2\text{O})_4$ ⁷⁸ and the lowest-energy geometry of $\text{K}^+(\text{H}_2\text{O})_3$.³⁶ Thus, the hydrated ammonium cluster, $\text{NH}_4^+(\text{H}_2\text{O})_3$, may have some attributes similar to those of pure water clusters and the monovalent $\text{K}^+(\text{H}_2\text{O})_3$ cation. The least stable isomer, **3c**, has a geometry similar to the *cis* and *trans* Zundel isomers of O_4H_9^+ cations which were also found to be relatively unstable among their isomers.³³

3a has a VEA of 2.943 eV and its Dyson orbital is an *s*-like function which chiefly resides outside the positions of the non-bridging protons. The Dyson orbital of isomer **3b** (VEA = 2.846 eV) is totally symmetric with its largest amplitudes beyond the non-bridging protons in the NH_4^+ fragment. For **3c**, whose VEA is 2.917 eV, the *s*-like Dyson orbital covers the NH_4^+ fragment and the water molecules directly bonded to it. All three $\text{NH}_4^+(\text{H}_2\text{O})_3$ isomers have VEAs that are ~0.3–0.5 eV lower than those of the $\text{NH}_4^+(\text{H}_2\text{O})_2$ isomers.

$\text{NH}_4^+(\text{H}_2\text{O})_4$ isomers:

Figure 4 displays the five isomers (**4a–4e**) of $\text{NH}_4^+(\text{H}_2\text{O})_4$ and their Dyson orbitals of electron attachment. In **4a**, the ammonium cation and three water molecules form two N-H---O and two O-H---O hydrogen bonds that constitute a ring whose structure is similar to an arrangement found in one of the isomers of $\text{O}_5\text{H}_{11}^+$.³³ Hydrogen bonds with O-H separations of 1.6753 Å and 1.831 Å pertain respectively to the upper (N-H---O) and lower (O-H---O) pairs of bridges that occur in the ring. The hydrogen bond outside the ring has a length of 1.7326 Å. **4a** has a VEA of 2.705 eV with a quasi-spherical Dyson orbital that spreads over the non-bridging protons in the ring subunit with its maximum amplitude on the NH_4^+ fragment.

Adding a water molecule that bridges between two of the water molecules of **3b** leads to the formation of isomer **4b**. All hydrogen bonds with the NH_4^+ fragment have lengths of 1.7872 Å. This isomer has a VEA of 2.581 eV and its Dyson orbital resides predominantly outside the positions of the non-bridging protons.

Isomer **4c** has a prism ring geometry similar to the prism ring isomer of $\text{O}_5\text{H}_{11}^+$.³³ This isomer has a VEA of 2.741 eV with a diffuse *s*-like Dyson orbital that spreads over the non-bridging protons. In isomer **4d**, a **3b** fragment with an approximate C_3 axis has a water molecule that lies in the second solvation shell. The **4d** isomer has a VEA of 2.599 eV and its Dyson orbital is distributed outside the exterior protons in the $\text{NH}_4^+(\text{H}_2\text{O})_3$ fragment.

Some studies^{36,39,74,75,77} have noted **4e** as the global minimum in perfect agreement with our data in Table I, which favors **4e** as the lowest energy isomer, i.e., the global minimum. In the **4e** geometry, the length of the H bond that links the water molecules to the NH_4^+ fragment is 1.8194 Å. This isomer

has a tetracoordinated geometry, with the four water molecules individually bound to each hydrogen center on the ammonium core. This high-symmetry isomer resembles the tetracoordinated isomers of $\text{Li}^+(\text{H}_2\text{O})_4$ and $\text{Na}^+(\text{H}_2\text{O})_4$ reported in preceding studies.³⁶ This particularly interesting tetracoordinated isomer (**4e**) validates the data from free-jet expansion experiments³⁵ in which three $\text{NH}_4^+(\text{H}_2\text{O})_n$ isomer classes were found, with a clear peak in the distribution and clusters of four, five and six water molecules being the most abundant. Thus, the dominant peak seen for $n = 4$ ³⁵ most likely corresponds to the S_4 point group. The S_4 point group was obtained as global minimum for $\text{Li}^+(\text{H}_2\text{O})_4$, $\text{Na}^+(\text{H}_2\text{O})_4$ and $\text{NH}_4^+(\text{H}_2\text{O})_4$ in previous *ab initio* calculations on monovalent-cation water clusters.³⁶ Similar conclusions were reached in theoretical¹⁶ and experimental¹³ studies based on $\text{NH}_4^+(\text{NH}_3)_4$ clusters. Isomer **4e** has a VEA of 2.581 eV. The totally symmetric, diffuse Dyson orbital (see red contour) that resides beyond the non-bridging protons is orthogonal to valence s functions of the oxygens and nitrogen nuclei. Overall, it is evident from Table I that with increasing n in $\text{NH}_4^+(\text{H}_2\text{O})_n$, the VEAs also decrease, thus enhancing super-alkali character.⁷⁶

3.2 Radical Excitation Energies and Dyson Orbitals of $\text{NH}_4(\text{H}_2\text{O})_n$ Rydberg Molecules

In anion photoelectron spectroscopy on DRAs, the final state of the doublet Rydberg radical may be an excited state instead of the ground-state. The excited states may be reached via simultaneous detachment of an electron from the Dyson orbital (of the lowest electron detachment energy) of the DRA and excitation from the same orbital to a more diffuse function, i.e., through a shakeup process. Convincing examples have been reported in the spectra¹⁴ of $\text{N}_n\text{H}_{3n+1}^-$ DRAs (for $n = 4-6$), where higher VEDEs were assigned to excited states of the doublet Rydberg radical and confirmed by EPT calculations.¹⁶ Several shakeup states that correspond to excitation energies of the Rydberg neutrals can easily be accessed by calculating VEAs of the closed shell cations. The vertical excitation energies of the doublet Rydberg radicals are inferred from differences between the VEAs as shown in Tables S10-S11 of ESI.

To guide experimentation, we have calculated several radical excitation energies for the highly symmetric systems that may dominate anion photoelectron spectra. For **3b** $\text{NH}_4^+(\text{H}_2\text{O})_3$ where the C_3 point group is obtained, several electron affinities of the cation corresponding to orbitals of higher angular momentum have been calculated. Vertical excitation energies thus inferred are displayed in Table II. All VEAs have pole strengths near unity. Excitation energies obtained with all the diagonal EPT methods are in close agreement. Dyson orbitals that correspond to several electron affinities are shown in Figure 5. The excited states occupy delocalized Dyson orbitals with s , p , d , and f nodal patterns that are orthogonalized to the N-H and O-H bond functions. Several excited states are doubly degenerate (2E), and the remaining counterparts belong to the 2A state. All the bound excited states shown in the P3+ EEs column of Table II range from 0.694 to 2.248 eV. The approximate l quantum numbers are based on the angular nodes of the Dyson orbitals corresponding to electron affinities of the cations as displayed in Figure 5.

For the tetracoordinated geometry of **4e** $\text{NH}_4^+(\text{H}_2\text{O})_4$, several electron affinities of the cation corresponding to orbitals of higher angular momentum have been calculated. Their vertical excitation energies are listed in Table III. Here also, the delocalized Dyson orbitals displayed in Figure 6 typify p -, d -, and f -like nodal patterns with orthogonalizations to the N-H and O-H bond functions. The P3+ excitation energies lie within 0.578 to 1.983 eV. The contours of the Dyson orbitals in Figure 6 (and their Aufbau principle) are similar to those observed in $\text{N}_n\text{H}_{3n+1}$ and $\text{O}_n\text{H}_{2n+1}$ Rydberg neutrals as well

as solvated electron precursors.^{16,30,32,33} Excited states of both radicals (**3b** $\text{NH}_4^+(\text{H}_2\text{O})_3$ and **4e** $\text{NH}_4^+(\text{H}_2\text{O})_4$) correspond to anion VEDEs below 2.5 eV and may be detectable in photoelectron experiments.

3.3 Isomers, Relative Energies, Vertical Electron Detachment Energies, and Dyson Orbitals of $\text{NH}_4^-(\text{H}_2\text{O})_n$ Double Rydberg Anions

Table IV presents various isomers and their relative energies that pertain to $\text{NH}_4^-(\text{H}_2\text{O})_n$ ($n=1-4$) DRAs. It is evident that for all values of n , the hydride–molecule complex is the most stable isomer. Similar conclusions were reached for DRAs based on nitrogen¹⁶ and oxygen³³. Isomerization energies obtained with lower levels of theory (Table S7) do not differ significantly from those obtained at the CCSD(T) plus MP2 zero-point corrections shown in Table IV. Only results from the latter method are discussed in the text.

Results for the lowest VEDEs obtained at the uncorrelated (KT) level and with various diagonal self-energy approximations (D2, D3, OVGf, P3 and P3+) are reported in Table S8. In most cases, VEDEs calculated with EPT methods that retain only the diagonal self-energy matrix elements have pole strengths below 0.85. OVGf results are unencouraging and therefore not recommended for studies on DRAs as earlier noted in studies on $\text{O}_n\text{H}_{2n+1}^-$ DRAs.³³ When pole strengths are below 0.85, electron binding energies and associated Dyson orbitals of diagonal self-energy approximations should be treated with caution. Thus, approximations that retain the full self-energy matrix are convenient for such instances.

To facilitate reliable prediction of VEDEs, pole strengths and corresponding Dyson orbitals, we made use of the non-diagonal BD-T1^{50,61-63} approximation, and the resulting data are included in Table IV. In BD-T1, all matrix blocks of the super-operator Hamiltonian that occur in the hole (h), particle (p), two-hole-one-particle (2hp) and two-particle-one-hole (2ph) operator manifolds are explicitly evaluated except the second-order couplings between 2ph and 2hp operators. The BD-T1 approximation employs the Brueckner doubles (BD) reference determinant⁷⁹⁻⁸¹ and its doubly excited amplitudes instead of the Hartree-Fock reference state. In addition to predicting high-accuracy VEDEs, Dyson orbitals from BD-T1 have better qualitative features than canonical molecular orbitals.⁶¹ Hence, only VEDEs obtained with the BD-T1 method are discussed in the text.

To judge the reliability of the VEDEs predicted with EPT methods, we performed $\Delta\text{CCSD(T)}$ estimations of VEDEs with the d-aug-cc-pVTZ basis set and the results are also presented in Table IV. Optimized geometries and Dyson orbitals of the DRAs are displayed in Figures 7–10. Note that all the reported Dyson orbitals are based on the highly accurate BD-T1 approximation. VEDEs obtained at the BD-T1 level agree closely with those from indirect $\Delta\text{CCSD(T)}$ calculations. (Detailed results for the indirect coupled-cluster methods are reported in Table S9). Note that throughout this section on anions, $\text{H}^-(\text{NH}_3)_n$ denotes hydride molecule complexes, $[\text{NH}_4^-](\text{H}_2\text{O})_n$ designates NH_4^- DRA-water complexes without NH-O bridges, and $\text{NH}_4^-(\text{H}_2\text{O})_n$ corresponds to micro-solvated DRAs that form H bridges with water molecules.

$\text{NH}_4^-(\text{H}_2\text{O})$ isomers:

For $n=1$, three isomers are obtained as displayed in Figure 7. In the $\text{H}^-(\text{NH}_3)\text{H}_2\text{O}$ complex, the hydride anion is weakly coordinated by the ammonia and water molecules, but this structure is the most stable. The predicted VEDE is near 2 eV. Given the high stability of this complex, a dominant

peak near this range is anticipated in anion photoelectron spectra. The Dyson orbital of this complex is chiefly a totally symmetric s -function on the hydride's nucleus that displays anti-bonding relationships with N-H and O-H bond functions. The optimized geometry suggests that H^- has a stronger attraction towards the water molecule than the ammonia molecule. Thus, the VEDE of the free H^- (0.75 eV) has been increased by electrostatic and other interactions with the solvent molecules.

In the next most stable isomer, an NH_4^- DRA-molecule complex is formed and denoted by $[\text{NH}_4^-]\text{H}_2\text{O}$. This complex has C_{2v} symmetry with a VEDE of 0.684 eV. The diffuse Dyson orbital is held at the periphery of the NH_4^- DRA with minor delocalization. The two radial nodes anticipate the 3s united-atom limit for the Dyson orbital. Alternative DRA-molecule structures composed of OH_3^- and NH_3 fragments rearrange without a barrier under optimization to the $[\text{NH}_4^-]\text{H}_2\text{O}$ minimum.

In the least stable **1a** $\text{NH}_4^-(\text{H}_2\text{O})$ isomer, a C_s cluster complex is obtained. The existing hydrogen bond between the N and O nuclei occurs at 1.8371 Å. The predicted VEDE of 0.495 eV is slightly above that of NH_4^- and N_2H_7^- ¹⁶ as well as slightly below those of OH_3^- and O_2H_5^- ³³ DRAs. The Dyson orbital is an approximately spherical function whose highest amplitudes occur beyond the non-bridging protons.

$\text{NH}_4^-(\text{H}_2\text{O})_2$ isomers:

The hydride-molecule complex retains its high stability upon addition of H_2O to form $\text{H}^-(\text{NH}_3)(\text{H}_2\text{O})_2$. The VEDE increases by 0.599 eV from the $\text{H}^-(\text{NH}_3)\text{H}_2\text{O}$ complex. Thus, addition of a water molecule increases the VEDE. This may be attributed to the stronger attraction of the H^- towards the water molecules than the ammonia. The totally symmetric diffuse Dyson orbital localizes near the H^- with slight anti-bonding relationships involving nearby solvent molecules.

In the $[\text{NH}_4^-](\text{H}_2\text{O})_2$ DRA-molecule complex from Figure 8, the NH_4^- DRA weakly interacts with the protons of the water molecules through electrostatic interactions in a C_{2v} arrangement. The VEDE is 0.886 eV. The Dyson orbital is a diffuse s -like function with two radial nodes and minor delocalization to neighboring solvent molecules.

The remaining two isomers, **2a** $\text{NH}_4^-(\text{H}_2\text{O})_2$ and **2b** $\text{NH}_4^-(\text{H}_2\text{O})_2$, are hydrogen-bonded DRA clusters. **2b** $\text{NH}_4^-(\text{H}_2\text{O})_2$ is more stable than **2a** $\text{NH}_4^-(\text{H}_2\text{O})_2$. In **2a** $\text{NH}_4^-(\text{H}_2\text{O})_2$, two of the protons of NH_4^- engage in hydrogen bonding with water molecules in a C_{2v} arrangement. **2b** $\text{NH}_4^-(\text{H}_2\text{O})_2$ has a discernable $\text{NH}_4^-(\text{H}_2\text{O})$ fragment interacting with an additional water molecule engaging in hydrogen bonding to form a water dimer. VEDEs of 0.539 and 0.552 eV, respectively, are obtained for the **2a** and **2b** isomers. Both isomers have Dyson orbitals whose maximum amplitudes lie beyond the non-bridging protons on the periphery of the complex, especially those associated with the NH_4^- fragment.

$\text{NH}_4^-(\text{H}_2\text{O})_3$ isomers:

For $n = 3$, five isomers are obtained: a hydride-molecule complex, a DRA-molecule complex, and three hydrogen-bonded DRA clusters as displayed in Figure 9. The hydride-molecule complex $\text{H}^-(\text{NH}_3)(\text{H}_2\text{O})_3$, emerges as the most stable isomer with a VEDE of 3.567 eV. Again, the new water molecule contributes to an increase in the VEDE. The Dyson orbital is a totally symmetric function centered chiefly on the hydride's nucleus that forms anti-bonding relationships with neighboring N-H and O-H bond functions.

In the next isomer, the NH_4^- DRA weakly interacts with the protons of the three water molecules to form the DRA-molecule $[\text{NH}_4^-](\text{H}_2\text{O})_3$ complex in which two H_2O molecules form a dimer. The VEDE is 1.075 eV, which is 0.189 eV higher than that of the $[\text{NH}_4^-](\text{H}_2\text{O})_2$ DRA-molecule complex. The Dyson orbital is a symmetric s -like function spread over the NH_4^- kernel with minimal delocalization.

The remaining three isomers are micro-solvated DRA clusters: **3a** $\text{NH}_4^-(\text{H}_2\text{O})_3$, **3b** $\text{NH}_4^-(\text{H}_2\text{O})_3$, and **3c** $\text{NH}_4^-(\text{H}_2\text{O})_3$. Of this set, **3c** is the most stable. **3a** and **3c** are ring structures that differ in relative orientations of their protons. **3b** retains its C_3 symmetry upon addition of two electrons to the **3b** $\text{NH}_4^+(\text{H}_2\text{O})_3$ cation. VEDEs near 0.5 eV are obtained for the three micro-solvated DRAs. The Dyson orbitals of **3a** and **3c** are diffused over the non-bridging protons. For **3b**, the pyramidal C_3 symmetry of its cation and anion yields a symmetric diffuse Dyson orbital that extends beyond the outer protons.

$\text{NH}_4^-(\text{H}_2\text{O})_4$ isomers:

Coordination of a water molecule through hydrogen bonding or electrostatic interactions to the five latter structures accounts for all seven isomers in Figure 10 when $n = 4$. The hydride cluster, $\text{H}^-(\text{NH}_3)(\text{H}_2\text{O})_4$, is the most stable with a large VEDE of 3.756 eV. The spherical Dyson orbital occupying the H^- ion also has some antibonding relationships with nearby N-H and O-H bond functions. The H^- ion is closer to the water molecules than to the ammonia molecule.

In the DRA-molecule complex, $[\text{NH}_4^-](\text{H}_2\text{O})_4$, the NH_4^- DRA is stabilized by a linear chain of four water molecules. With a VEDE of 1.177 eV, its Dyson orbital spreads over the NH_4^- fragment. Minor delocalization from the nearest H_2O is discernable, and the green contours arise from orthogonalization to the valence nitrogen functions with three radial nodes. The data of Table IV indicate that the DRA-molecule complex, $[\text{NH}_4^-](\text{H}_2\text{O})_4$, is the second most stable isomer.

The five remaining isomers, **4a-4e** $\text{NH}_4^-(\text{H}_2\text{O})_4$, are micro-solvated DRAs arising from the reduction of their respective cationic congeners. **4a** has a three-dimensional cage structure with C_s symmetry. **4e** has a tetracoordinate NH_4^- fragment joined to a water molecule that forms hydrogen bonds with another water molecule and the anionic center. Note that a tetracoordinate NH_4^- was identified in $\text{N}_n\text{H}_{3n+1}^-$ DRAs with similar geometric features.¹⁶ All the micro-solvated DRAs have VEDEs near 0.5 eV. The diffuse s -like Dyson orbitals spread over the exterior nonbonding protons with orthogonalizations to the valence functions on the nitrogen and the oxygen nuclei. For **4e**, a symmetric Dyson orbital whose amplitudes in green surround the peripheral protons displays nodes that result in red s -like contours on the N and O centers.¹⁶

4. CONCLUSIONS

A new family of DRAs that is based on micro-solvation of tetrahedral NH_4^- by one to four water molecules has been identified and its VEDEs and corresponding Dyson orbitals have been predicted. *Ab initio* electron-propagator (i.e., direct) and coupled-cluster (i.e., indirect) methods have been employed to predict electron binding energies of cationic, radical and anionic species. Several approximate electron propagator methods predict VEDEs that are in close agreement with those obtained with $\Delta\text{CCSD(T)}$. The BD-T1 method predicts the most reliable VEDEs. Vertical electron attachment energies (VEAEs) of $\text{NH}_4^+(\text{H}_2\text{O})_n$ ($n = 1-4$) cationic clusters were calculated with the

direct and indirect methods. The VEAEs decrease with increasing n and the corresponding Dyson orbitals are diffused over peripheral, non-hydrogen bonded protons.

Clusters formed from NH_4^- DRAs and stabilized by hydrogen bonding or electrostatic interactions are less stable than $\text{H}^-(\text{NH}_3)(\text{H}_2\text{O})_n$ isomers. For all values of n , the hydride-molecule complex $\text{H}^-(\text{NH}_3)(\text{H}_2\text{O})_n$ is always the most stable and has the largest VEDEs. DRAs formed from electrostatic interactions between NH_4^- and water molecules, denoted by $[\text{NH}_4^-](\text{H}_2\text{O})_n$, are more stable than the $\text{NH}_4^-(\text{H}_2\text{O})_n$ DRAs that exhibit NH-O hydrogen bridges. The latter species have VEDEs near 0.5 eV and therefore resemble the original DRAs. Variations in these VEDEs are consequences of distinct coordination environments that include proton donations by the tetrahedral anion to water molecules. Whereas total energies of $\text{N}_n\text{H}_{3n+1}^-$ ¹⁶ and $\text{O}_n\text{H}_{2n+1}^-$ ³³ DRAs favor formation of H bonds, the opposite trend emerges for the present systems. An increasing sequence of larger, well-separated VEDEs for the $[\text{NH}_4^-](\text{H}_2\text{O})_n$ DRAs, wherein the tetrahedral NH_4^- fragment interacts with water molecules without formation of H bridges, has been established. Dyson orbitals of electron attachment to $\text{NH}_4^+(\text{H}_2\text{O})_n$ cations and of detachment from $\text{NH}_4^-(\text{H}_2\text{O})_n$ DRAs occupy regions beyond the exterior non-bridging O-H and N-H bonds. Thus, the Rydberg electrons in the uncharged Rydberg radicals and DRAs are held near the outer protons of the water and ammonia molecules. The low-lying excited states of the doublet Rydberg radicals have a single electron occupying extended s -like, p -like, d -like, or f -like Dyson orbitals with the following Aufbau principle: 1s, 1p, 1d, 2s, 2p, 1f. As $\text{NH}_4^-(\text{H}_2\text{O})_n$ DRAs isomers have well separated VEDEs and experimentally accessible total energies, they are expected to appear in mass-selected, anion photoelectron spectra that typically detect low-lying isomers.

Data Availability Statement

The data that support the findings of this study are available within the manuscript and the electronic supporting information (ESI). The ESI contains the Cartesian coordinates of all optimized cationic and anionic geometries. Appropriate Tables that support the findings in his study are also included. Sample input files for electron propagator theory calculations are provided in the ESI as well.

Funding

This work was supported by the National Science Foundation via grant CHE-1565760 to Auburn University.

Acknowledgment

The authors thank the Alabama Supercomputer Center for computing resources.

REFERENCES

- 1 J. T. Snodgrass, J. V. Coe, C. B. Freidhoff, K. M. McHugh and K. H. Bowen, *Faraday Discuss. Chem. Soc.*, 1988, **86**, 241–256.
- 2 J. V. Coe, J. T. Snodgrass, C. B. Freidhoff, K. M. McHugh and K. H. Bowen, *J. Chem. Phys.*, 1985, **83**, 3169–3170.
- 3 G. Herzberg and J. T. Hougen, *J. Mol. Spectrosc.*, 1983, **97**, 430–440.
- 4 J. V. Ortiz, *J. Chem. Phys.*, 1988, **89**, 6348–6352.
- 5 D. Cremer and E. Kraka, *J. Phys. Chem.*, 1986, **90**, 33–40.

- 6 H. Cardy, C. Larrieu and A. Dargelos, *Chem. Phys. Lett.*, 1986, **131**, 507–512.
- 7 J. V. Ortiz, *J. Chem. Phys.*, 1987, **87**, 3557–3562.
- 8 M. Gutowski, J. Simons, R. Hernandez and H. L. Taylor, *J. Phys. Chem.*, 1988, **92**, 6179–6182.
- 9 M. Gutowski and J. Simons, *J. Chem. Phys.*, 1990, **93**, 3874–3880.
- 10 J. Simons and M. Gutowski, *Chem. Rev.*, 1991, **91**, 669–677.
- 11 J. Wang and R. J. Boyd, *Can. J. Phys.*, 1994, **72**, 851–855.
- 12 N. Matsunaga and M. S. Gordon, *J. Phys. Chem.*, 1995, **99**, 12773–12780.
- 13 S. J. Xu, J. M. Nilles, J. H. Hendricks, S. A. Lyapustina and K. H. Bowen, *J. Chem. Phys.*, 2002, **117**, 5742–5747.
- 14 D. Radisic, S. T. Stokes and K. H. Bowen, *J. Chem. Phys.*, 2005, **123**, 011101.
- 15 J. V. Ortiz, *J. Chem. Phys.*, 2002, **117**, 5748–5756.
- 16 M. Díaz-Tinoco and J. V. Ortiz, *J. Chem. Phys.*, 2019, **151**, 054301.
- 17 M. Díaz-Tinoco and J. V. Ortiz, *J. Phys. Chem. A*, 2019, **123**, 10961–10967.
- 18 H. Hopper, M. Lococo, O. Dolgounitcheva, V. G. Zakrzewski and J. V. Ortiz, *J. Am. Chem. Soc.*, 2000, **122**, 12813–12818.
- 19 J. V. Ortiz, *J. Chem. Phys.*, 1989, **91**, 7024–7029.
- 20 J. Melin and J. V. Ortiz, *J. Chem. Phys.*, 2007, **127**, 014307.
- 21 J. V. Ortiz, *J. Phys. Chem.*, 1990, **94**, 4762–4763.
- 22 J. Melin, G. Seabra and J. V. Ortiz, *Theor. Comput. Chem.*, 2007, **19**, 87–100.
- 23 A. I. Boldyrev and J. Simons, *J. Chem. Phys.*, 1998, **97**, 6621.
- 24 I. Anusiewicz, S. Freza, M. Bobrowski and P. Skurski, *J. Chem. Phys.*, 2021, **154**, 104302.
- 25 R. Barrios, P. Skurski and J. Simons, *J. Phys. Chem. A*, 2000, **104**, 10855–10858.
- 26 M. V. Ivanov, A. I. Krylov and S. Zilberg, *J. Phys. Chem. Lett.*, 2020, **11**, 2284–2290.
- 27 R. Riedel, A. G. Seel, D. Malko, D. P. Miller, B. T. Sperling, H. Choi, T. F. Headen, E. Zurek, A. Porch, A. Kucernak, N. C. Pyper, P. P. Edwards and A. G. M. Barrett, *J. Am. Chem. Soc.*, 2021, **143**, 3934–3943.
- 28 I. Anusiewicz, P. Skurski and J. Simons, *J. Phys. Chem. B*, 2014, **118**, 7892–7901.
- 29 J. P. Simons, *J. Chem. Phys.*, 2022, **156**, 100901.
- 30 I. R. Ariyaratna, S. N. Khan, F. Pawłowski, J. V. Ortiz and E. Miliordos, *J. Phys. Chem. Lett.*, 2018, **9**, 84–88.
- 31 I. R. Ariyaratna, F. Pawłowski, J. V. Ortiz and E. Miliordos, *Phys. Chem. Chem. Phys.*, 2018, **20**, 24186–24191.
- 32 I. R. Ariyaratna, F. Pawłowski, J. V. Ortiz and E. Miliordos, *J. Phys. Chem. A*, 2020, **124**, 505–512.
- 33 E. Opoku, F. Pawłowski and J. V. Ortiz, *J. Chem. Phys.*, 2021, **154**, 234304.
- 34 S. T. Pei, S. Jiang, Y. R. Liu, T. Huang, K. M. Xu, H. Wen, Y. P. Zhu and W. Huang, *J. Phys. Chem. A*, 2015, **119**, 3035–3047.
- 35 Y. S. Wang, H. C. Chang, J. C. Jiang, S. H. Lin, Y. T. Lee and H. C. Chang, *J. Am. Chem. Soc.*, 1998, **120**, 8777–8788.
- 36 H. M. Lee, P. Tarakeshwar, J. Park, M. R. Kołaski, Y. Jin Yoon, H. B. Yi, W. Y. Kim and K. S. Kim, *J. Phys. Chem. A*, 2004, **108**, 2949–2958.
- 37 S. Karthikeyan, J. N. Singh, M. Park, R. Kumar and K. S. Kim, *J. Chem. Phys.*, 2008, **128**, 5648.
- 38 J. Douady, F. Calvo and F. Spiegelman, *J. Chem. Phys.*, 2008, **129**, 154305.
- 39 Y. L. Zhao, M. Meot-Ner and C. Gonzalez, *J. Phys. Chem. A*, 2009, **113**, 2967–2974.
- 40 T. E. Morreis and G. C. Shields, *J. Phys. Chem. A*, 2010, **114**, 4266–4271.
- 41 R. P. Wayne, *Chemistry of atmospheres*, Oxford University Press, Oxford, UK, 1991.
- 42 E. N. Baker and R. E. Hubbard, *Prog. Biophys. Mol. Biol.*, 1984, **44**, 97–179.
- 43 G. W. Robinson, P. J. Thistlethwaite and J. Lee, *J. Phys. Chem.*, 1986, **90**, 4224–4233.

- 44 R. Ludwig, *Angew. Chemie - Int. Ed.*, 2001, **40**, 1808–1827.
- 45 J. Linderberg and Y. Öhrn, *Propagators in Quantum Chemistry*, John Wiley & Sons, Inc., Hoboken, NJ, USA, 2004.
- 46 H. H. Corzo and J. V. Ortiz, in *Advances in Quantum Chemistry*, Academic Press Inc., 2017, vol. 74, pp. 267–298.
- 47 J. V. Ortiz, in *Annual Reports in Computational Chemistry*, Elsevier Ltd, 2017, vol. 13, pp. 139–182.
- 48 T. Koopmans, *Physica*, 1934, **1**, 104–113.
- 49 J. V. Ortiz, *Int. J. Quantum Chem.*, 2005, **105**, 803–808.
- 50 J. V. Ortiz, *Wiley Interdiscip. Rev. Comput. Mol. Sci.*, 2013, **3**, 123–142.
- 51 W. von Niessen, J. Schirmer and L. S. Cederbaum, *Comput. Phys. Reports*, 1984, **1**, 57–125.
- 52 L. S. Cederbaum, *J. Phys. B At. Mol. Phys.*, 1975, **8**, 290–303.
- 53 V. G. Zakrzewski, J. V. Ortiz, J. A. Nichols, D. Heryadi, D. L. Yeager and J. T. Golab, *Int. J. Quantum Chem.*, 1996, **60**, 29–36.
- 54 J. V. Ortiz, in *Computational Chemistry: Reviews of Current*, World Scientific, 1997, pp. 1–61.
- 55 J. V. Ortiz, *J. Chem. Phys.*, 1996, **104**, 7599–7605.
- 56 V. G. Zakrzewski, O. Dolgounitcheva, A. V. Zakjevskii and J. V. Ortiz, *Int. J. Quantum Chem.*, 2010, **110**, 2918–2930.
- 57 V. G. Zakrzewski, O. Dolgounitcheva, A. V. Zakjevskii and J. V. Ortiz, in *Annual Reports in Computational Chemistry*, Elsevier BV, 2010, vol. 6, pp. 79–94.
- 58 V. G. Zakrzewski, O. Dolgounitcheva, A. V. Zakjevskii and J. V. Ortiz, in *Advances in Quantum Chemistry*, Academic Press Inc., 2011, vol. 62, pp. 105–136.
- 59 E. Opoku, F. Pawłowski and J. V. Ortiz, *J. Chem. Phys.*, 2021, **155**, 204107.
- 60 M. Díaz-Tinoco, H. H. Corzo, F. Pawłowski and J. V. Ortiz, *Mol. Phys.*, 2019, **117**, 2275–2283.
- 61 J. V. Ortiz, *J. Chem. Phys.*, 2020, **153**, 070902.
- 62 J. V. Ortiz, *J. Chem. Phys.*, 1998, **109**, 5741–5746.
- 63 J. V. Ortiz, *Int. J. Quantum Chem.*, 1999, **75**, 615–621.
- 64 T. H. Dunning, *J. Chem. Phys.*, 1989, **90**, 1007–1023.
- 65 R. A. Kendall, T. H. Dunning and R. J. Harrison, *J. Chem. Phys.*, 1992, **96**, 6796–6806.
- 66 G. D. Purvis and R. J. Bartlett, *J. Chem. Phys.*, 1982, **76**, 1910–1918.
- 67 K. Raghavachari, G. W. Trucks, J. A. Pople and M. Head-Gordon, *Chem. Phys. Lett.*, 1989, **157**, 479–483.
- 68 D. E. Woon and T. H. Dunning, *J. Chem. Phys.*, 1994, **100**, 2975–2988.
- 69 M. J. Frisch, G. W. Trucks, H. B. Schlegel, G. E. Scuseria, M. A. Robb, J. R. Cheeseman, G. Scalmani, V. Barone, G. A. Petersson, H. Nakatsuji, X. Li, M. Caricato, A. V. Marenich, J. Bloino, B. G. Janesko, R. Gomperts, B. Mennucci, H. P. Hratchian, J. V. Ortiz, A. F. Izmaylov, J. L. Sonnenberg, D. Williams-Young, F. Ding, F. Lipparini, F. Egidi, J. Goings, B. Peng, A. Petrone, T. Henderson, D. Ranasinghe, V. G. Zakrzewski, J. Gao, N. Rega, G. Zheng, W. Liang, M. Hada, M. Ehara, K. Toyota, R. Fukuda, J. Hasegawa, M. Ishida, T. Nakajima, Y. Honda, O. Kitao, H. Nakai, T. Vreven, K. Throssell, J. A. Montgomery Jr., J. E. Peralta, F. Ogliaro, M. J. Bearpark, J. J. Heyd, E. N. Brothers, K. N. Kudin, V. N. Staroverov, T. A. Keith, R. Kobayashi, J. Normand, K. Raghavachari, A. P. Rendell, J. C. Burant, S. S. Iyengar, J. Tomasi, M. Cossi, J. M. Millam, M. Klene, C. Adamo, R. Cammi, J. W. Ochterski, R. L. Martin, K. Morokuma, O. Farkas, J. B. Foresman and D. J. Fox, 2016, Gaussian 16, Revision A.01, Gaussian, Inc., Wallingford, CT.
- 70 M. J. Frisch, G. W. Trucks, H. B. Schlegel, G. E. Scuseria, M. a. Robb, J. R. Cheeseman, G. Scalmani, V. Barone, G. a. Petersson, H. Nakatsuji, X. Li, M. Caricato, a. V. Marenich, J. Bloino, B. G. Janesko, R. Gomperts, B. Mennucci, H. P. Hratchian, J. V. Ortiz, a. F. Izmaylov,

- J. L. Sonnenberg, Williams, F. Ding, F. Lipparini, F. Egidi, J. Goings, B. Peng, A. Petrone, T. Henderson, D. Ranasinghe, V. G. Zakrzewski, J. Gao, N. Rega, G. Zheng, W. Liang, M. Hada, M. Ehara, K. Toyota, R. Fukuda, J. Hasegawa, M. Ishida, T. Nakajima, Y. Honda, O. Kitao, H. Nakai, T. Vreven, K. Throssell, J. a. Montgomery Jr., J. E. Peralta, F. Ogliaro, M. J. Bearpark, J. J. Heyd, E. N. Brothers, K. N. Kudin, V. N. Staroverov, T. a. Keith, R. Kobayashi, J. Normand, K. Raghavachari, a. P. Rendell, J. C. Burant, S. S. Iyengar, J. Tomasi, M. Cossi, J. M. Millam, M. Klene, C. Adamo, R. Cammi, J. W. Ochterski, R. L. Martin, K. Morokuma, O. Farkas, J. B. Foresman and D. J. Fox, 2018, Gaussian Development Version, Revision 1.14, Gaussian, Inc., Wallingford, CT.
- 71 R. Dennington, T. A. Keith and J. M. Millam, 2019, GaussView, Version 6.1, Semichem Inc., Shawnee Mission, KS.
- 72 G. Schaftenaar and J. H. Noordik, *J. Comput. Aided. Mol. Des.*, 2000, **14**, 123–134.
- 73 A. Malloum, J. J. Fifen and J. Conradie, *J. Chem. Phys.*, 2018, **149**, 244301.
- 74 F. C. Pickard IV, M. E. Dunn and G. C. Shields, *J. Phys. Chem. A*, 2005, **109**, 4905–4910.
- 75 J. C. Jiang, *J. Phys. Chem. A*, 1999, **103**, 3123–3135.
- 76 G. L. Gutsev and A. I. Boldyrev, *Chem. Phys. Lett.*, 1982, **92**, 262–266.
- 77 F. Zhao, C. Liu, L. Gong and Z. Yang, *Acta Chim. Sin.*, 2011, **69**, 1147–1150.
- 78 S. S. Xantheas, *Chem. Phys.*, 2000, **258**, 225–231.
- 79 K. A. Brueckner, *Phys. Rev.*, 1954, **96**, 508.
- 80 R. K. Nesbet, *Phys. Rev.*, 1958, **109**, 1632.
- 81 N. C. Handy, J. A. Pople, M. Head-Gordon, K. Raghavachari and G. W. Trucks, *Chem. Phys. Lett.*, 1989, **164**, 185–192.

Table I: $\text{NH}_4^+(\text{H}_2\text{O})_n$ isomerization^a and vertical electron attachment energies (VEAEs). Pole strengths are in parentheses. All energies are in eV.
^aIsomerization energies in third column are obtained at the CCSD(T) with MP2 zero-point energy corrections.

<i>n</i>	Isomer	$\Delta E_{MP2-ZPE}^{CCSD(T)}$	KT	D2	D3	OVGF-A	OVGF-B	OVGF-C	P3	P3+	$\Delta\text{CCSD(T)}$
1	1a $\text{NH}_4^+(\text{H}_2\text{O})$	-	3.324	3.744(0.988)	3.722(0.987)	3.725 (0.987)	3.726 (0.986)	3.724 (0.986)	3.749 (0.986)	3.748 (0.986)	3.826
2	2a $\text{NH}_4^+(\text{H}_2\text{O})_2$	0.000	2.836	3.220(0.989)	3.217 (0.987)	3.218 (0.988)	3.221 (0.987)	3.217 (0.987)	3.226 (0.987)	3.226 (0.987)	3.332
	2b $\text{NH}_4^+(\text{H}_2\text{O})_2$	0.130	2.969	3.361(0.988)	3.348 (0.987)	3.350 (0.987)	3.352 (0.987)	3.349 (0.987)	3.368 (0.986)	3.367 (0.987)	3.456
3	3a $\text{NH}_4^+(\text{H}_2\text{O})_3$	0.047	2.569	2.937 (0.989)	2.940 (0.988)	2.940 (0.988)	2.944 (0.987)	2.939 (0.987)	2.943 (0.987)	2.943 (0.987)	3.071
	3b $\text{NH}_4^+(\text{H}_2\text{O})_3$	0.000	2.490	2.840 (0.990)	2.850 (0.988)	2.849 (0.988)	2.853 (0.988)	2.848 (0.988)	2.847 (0.988)	2.846 (0.988)	2.972
	3c $\text{NH}_4^+(\text{H}_2\text{O})_3$	0.096	2.554	2.910 (0.989)	2.915 (0.988)	2.915 (0.988)	2.918 (0.988)	2.914 (0.988)	2.917 (0.987)	2.917 (0.987)	3.033
4	4a $\text{NH}_4^+(\text{H}_2\text{O})_4$	0.088	2.362	2.698 (0.990)	2.706 (0.989)	2.705 (0.989)	2.709 (0.988)	2.705 (0.989)	2.706 (0.989)	2.705 (0.988)	2.834
	4b $\text{NH}_4^+(\text{H}_2\text{O})_4$	0.014	2.301	2.638 (0.990)	2.649 (0.989)	2.647 (0.989)	2.652 (0.988)	2.647 (0.988)	2.645 (0.988)	2.645 (0.988)	2.785
	4c $\text{NH}_4^+(\text{H}_2\text{O})_4$	0.133	2.385	2.734 (0.989)	2.742 (0.988)	2.740 (0.988)	2.745 (0.988)	2.741(0.988)	2.742 (0.987)	2.741 (0.988)	2.878
	4d $\text{NH}_4^+(\text{H}_2\text{O})_4$	0.067	2.269	2.591(0.990)	2.607 (0.989)	2.604 (0.989)	2.609 (0.989)	2.605 (0.989)	2.599 (0.988)	2.599 (0.988)	2.730
	4e $\text{NH}_4^+(\text{H}_2\text{O})_4$	0.000	2.256	2.574 (0.990)	2.591(0.989)	2.587 (0.989)	2.593 (0.989)	2.589 (0.989)	2.582 (0.988)	2.581(0.989)	2.715

Table II: First twenty radical excitation energies (EEs) of **3b** $\text{NH}_4^+(\text{H}_2\text{O})_3$. All energies are in eV. The numbers in second column refer to Figure 5.

<i>l</i>	Dyson #	Final State	KT EEs	D2 EEs	D3 EEs	OVGF-B EEs	P3 EEs	P3+ EEs
s	1	1 ² A	0.000	0.000	0.000	0.000	0.000	0.000
p	2,3	1 ² E	0.553	0.696	0.696	0.696	0.695	0.694
	4	2 ² A	0.626	0.828	0.827	0.828	0.828	0.828
d	5,6	2 ² E	1.113	1.363	1.367	1.367	1.364	1.364
	7	3 ² A	1.163	1.406	1.412	1.411	1.408	1.408
	8,9	3 ² E	1.244	1.533	1.536	1.535	1.535	1.534
s	10	4 ² A	1.339	1.579	1.586	1.585	1.584	1.583
p	11,12	4 ² E	1.610	1.849	1.855	1.854	1.853	1.852
	13	5 ² A	1.598	1.860	1.866	1.866	1.864	1.863
f	14,15	5 ² E	1.751	2.041	2.048	2.048	2.044	2.043
	16	6 ² A	1.855	2.141	2.146	2.145	2.143	2.143
	17,18	6 ² E	1.912	2.190	2.194	2.194	2.192	2.192
	19	7 ² A	1.998	2.241	2.248	2.247	2.244	2.244
	20	8 ² A	1.962	2.245	2.249	2.250	2.248	2.248

Table III: First eighteen and radical excitation energies (EEs) for $4e \text{ NH}_4^+(\text{H}_2\text{O})_4$. All energies are in eV. The numbers in second column refer to Figure 6.

<i>l</i>	Dyson #	Final State	KT EEs	D2 EEs	D3 EEs	OVSF-B EEs	P3 EEs	P3+ EEs
s	1	1^2A_1	0.000	0.000	0.000	0.000	0.000	0.000
p	2	1^2B	0.449	0.579	0.583	0.583	0.578	0.578
	3,4	1^2E	0.456	0.586	0.590	0.590	0.586	0.585
d	5	2^2B	0.945	1.168	1.178	1.177	1.170	1.170
	6,7	2^2E	0.966	1.192	1.202	1.202	1.195	1.194
	8	2^2A	1.020	1.272	1.281	1.279	1.274	1.274
	9	3^2B	1.066	1.326	1.335	1.333	1.329	1.328
s	10	3^2A	1.147	1.341	1.354	1.352	1.348	1.347
p	11,12	3^2E	1.403	1.633	1.645	1.644	1.638	1.638
	13	4^2B	1.444	1.646	1.657	1.656	1.651	1.650
d	14	4^2A	1.550	1.801	1.814	1.813	1.804	1.804
	15	5^2A	1.568	1.825	1.838	1.837	1.829	1.828
	16,17	4^2E	1.668	1.934	1.944	1.943	1.936	1.936
	18	5^2B	1.761	1.979	1.989	1.988	1.984	1.983

Table IV: $\text{NH}_4^-(\text{H}_2\text{O})_n$ isomers and their vertical electron detachment energies (VEDEs). Pole strengths are in parentheses. All energies are in eV. ^aIsomerization energies in third column are obtained at the CCSD(T) with MP2 zero-point energy corrections.

<i>n</i>	Isomer	$\Delta E_{\text{MP2-ZPE}}^{\text{CCSD(T)}}$	KT	D2	P3+	BD-T1	$\Delta\text{CCSD(T)}$
1	$\text{H}^-(\text{NH}_3)\text{H}_2\text{O}$	0.000	2.512	1.969 (0.893)	1.985 (0.908)	2.172 (0.882)	2.085
	$[\text{NH}_4^-]\text{H}_2\text{O}$	1.148	0.368	0.770 (0.877)	0.723 (0.854)	0.684 (0.881)	0.675
	1a $\text{NH}_4^-(\text{H}_2\text{O})$	1.194	0.211	0.575 (0.872)	0.517 (0.835)	0.495 (0.862)	0.491
2	$\text{H}^-(\text{NH}_3)(\text{H}_2\text{O})_2$	0.000	3.135	2.574 (0.903)	2.576 (0.908)	2.771 (0.831)	2.693
	$[\text{NH}_4^-](\text{H}_2\text{O})_2$	1.667	0.490	0.954 (0.881)	0.920 (0.866)	0.886 (0.894)	0.886
	2a $\text{NH}_4^-(\text{H}_2\text{O})_2$	1.641	0.186	0.607 (0.873)	0.558 (0.835)	0.539 (0.870)	0.553
	2b $\text{NH}_4^-(\text{H}_2\text{O})_2$	1.557	0.238	0.621 (0.862)	0.568 (0.829)	0.552 (0.864)	0.556
3	$\text{H}^-(\text{NH}_3)(\text{H}_2\text{O})_3$	0.000	3.980	3.352 (0.908)	3.364 (0.908)	3.567 (0.900)	3.470
	$[\text{NH}_4^-](\text{H}_2\text{O})_3$	1.923	0.632	1.138 (0.886)	1.112 (0.874)	1.075 (0.899)	1.081
	3a $\text{NH}_4^-(\text{H}_2\text{O})_3$	1.925	0.143	0.534 (0.860)	0.471 (0.812)	0.459 (0.856)	0.481
	3b $\text{NH}_4^-(\text{H}_2\text{O})_3$	1.971	0.169	0.575 (0.857)	0.513 (0.809)	0.498 (0.856)	0.517
	3c $\text{NH}_4^-(\text{H}_2\text{O})_3$	1.809	0.186	0.574 (0.863)	0.525 (0.827)	0.537 (0.868)	0.551
4	$\text{H}^-(\text{NH}_3)(\text{H}_2\text{O})_4$	0.000	4.192	3.543 (0.908)	3.551 (0.903)	3.756 (0.896)	3.659
	$[\text{NH}_4^-](\text{H}_2\text{O})_4$	2.061	0.730	1.240 (0.889)	1.213 (0.877)	1.177 (0.900)	1.183
	4a $\text{NH}_4^-(\text{H}_2\text{O})_4$	2.126	0.141	0.523 (0.861)	0.470 (0.817)	0.473 (0.860)	0.481
	4b $\text{NH}_4^-(\text{H}_2\text{O})_4$	2.195	0.148	0.522 (0.838)	0.452 (0.785)	0.432 (0.853)	0.439
	4c $\text{NH}_4^-(\text{H}_2\text{O})_4$	2.178	0.162	0.521 (0.840)	0.457 (0.795)	0.455 (0.858)	0.474
	4d $\text{NH}_4^-(\text{H}_2\text{O})_4$	2.264	0.173	0.586 (0.848)	0.529 (0.803)	0.515 (0.859)	0.530
	4e $\text{NH}_4^-(\text{H}_2\text{O})_4$	2.318	0.183	0.566 (0.839)	0.509 (0.799)	0.534 (0.863)	0.564

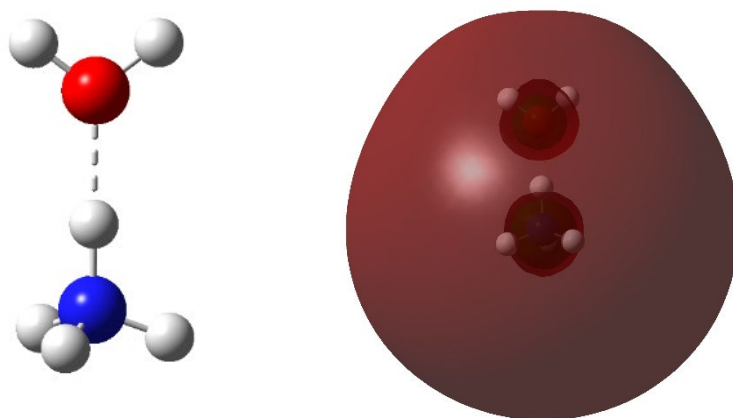


Figure 1: Optimized geometry and Dyson orbital of electron attachment to $\text{NH}_4^+(\text{H}_2\text{O})$.

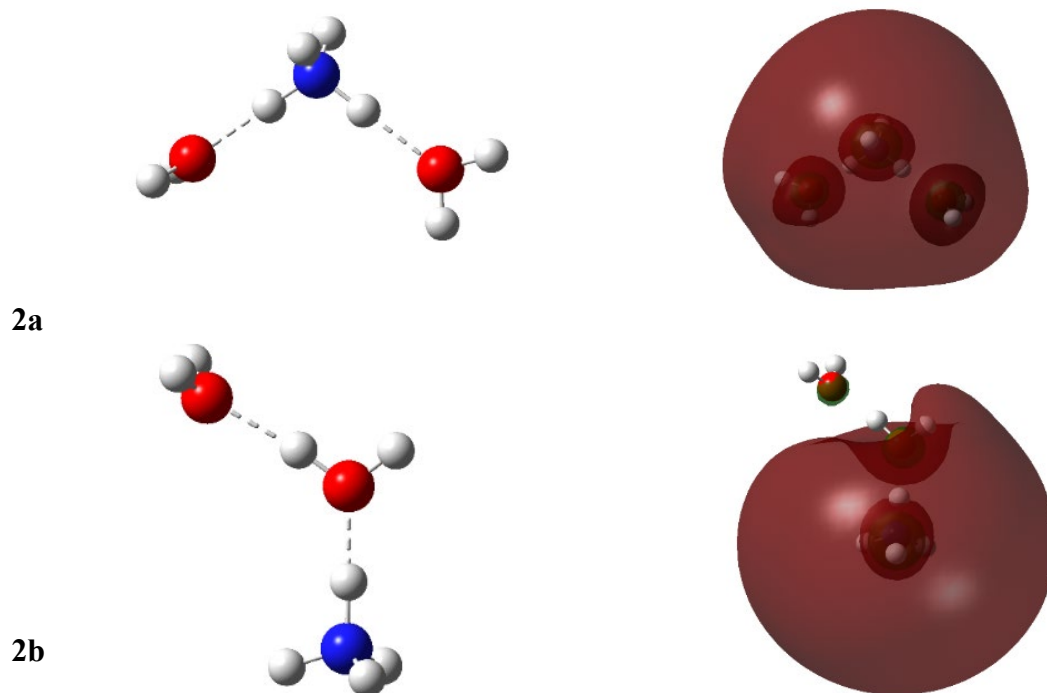


Figure 2: Optimized geometries and Dyson orbitals of electron attachment to $\text{NH}_4^+(\text{H}_2\text{O})_2$ cations.

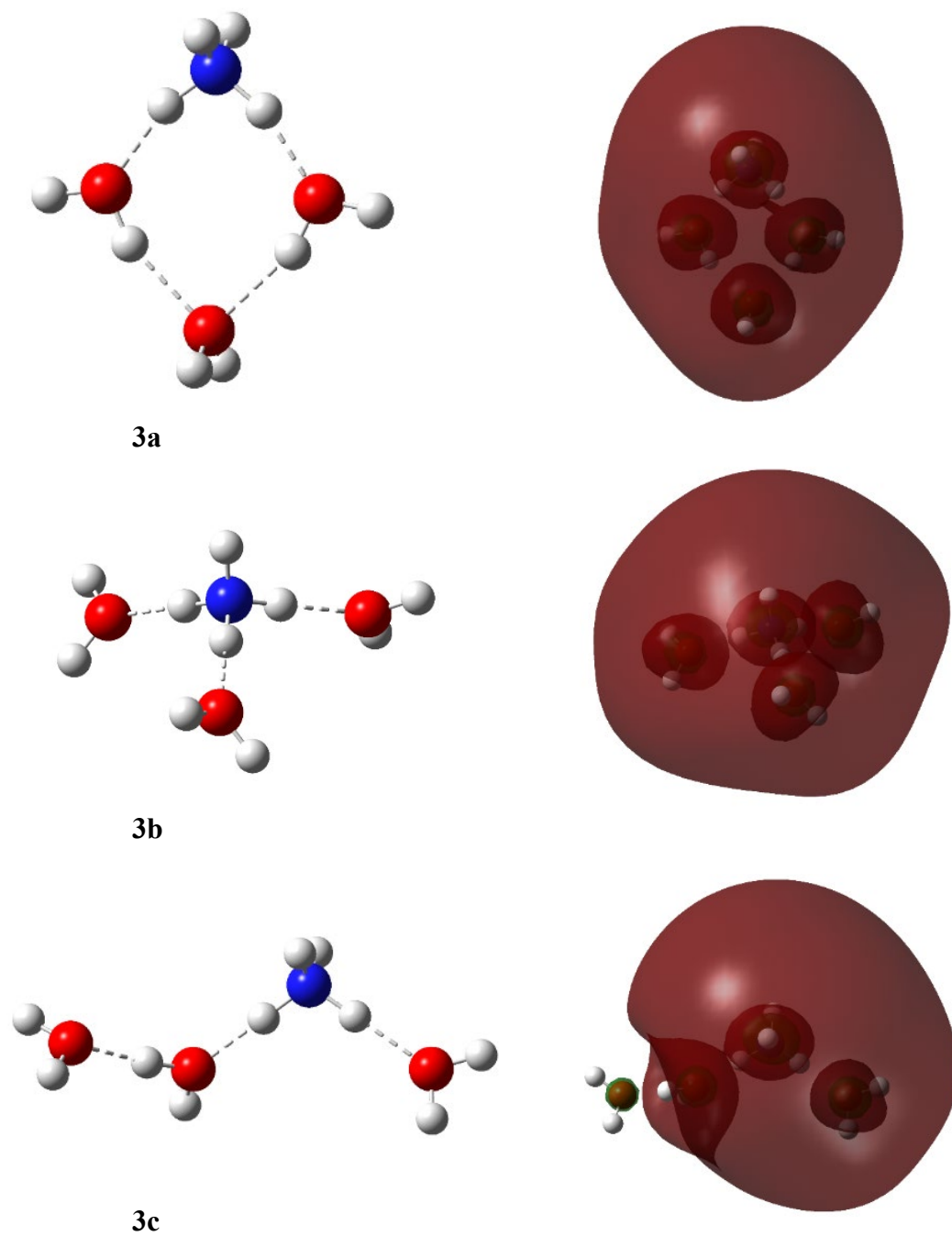


Figure 3: Optimized geometries and Dyson orbitals of electron attachment to $\text{NH}_4^+(\text{H}_2\text{O})_3$ cations.

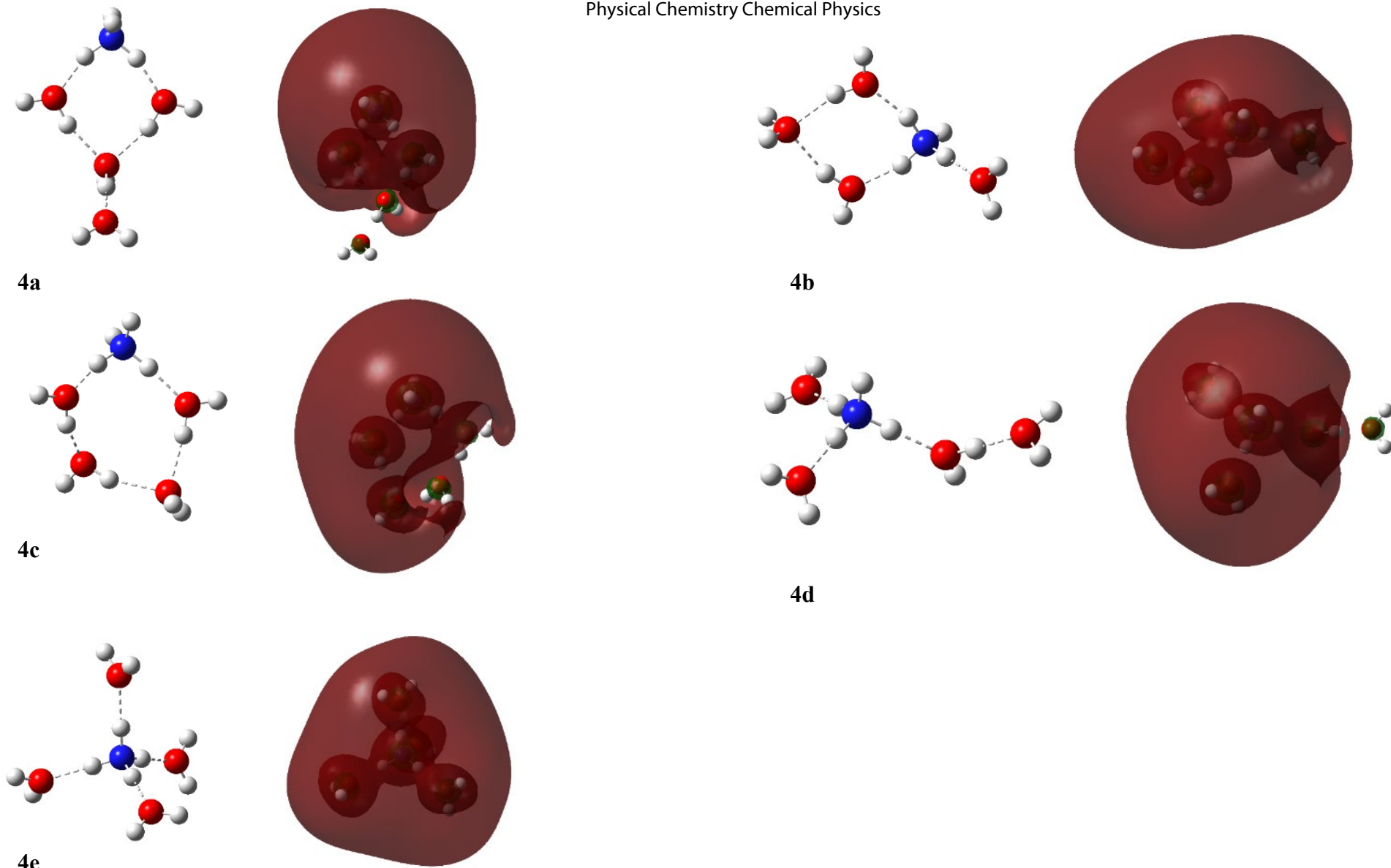


Figure 4: Optimized geometries and Dyson orbitals of electron attachment to $\text{NH}_4^+(\text{H}_2\text{O})_4$ cations.

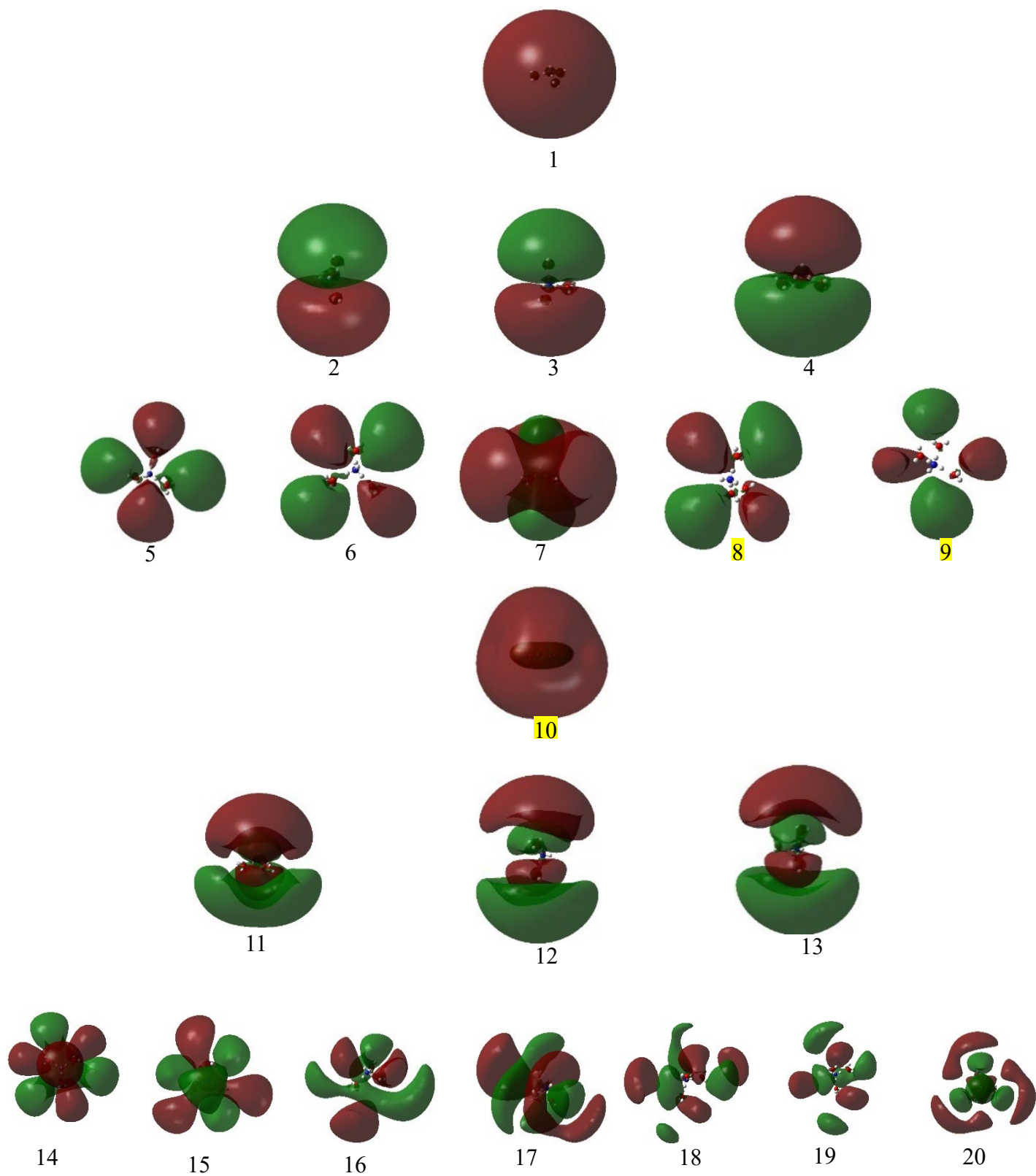


Figure 5: Dyson orbitals of electron attachment to the cation for ground and excited states of the $3b$ $\text{NH}_4(\text{H}_2\text{O})_3$ Rydberg radical. The numerical labels correspond to those in the second column of Table II (Dyson #).

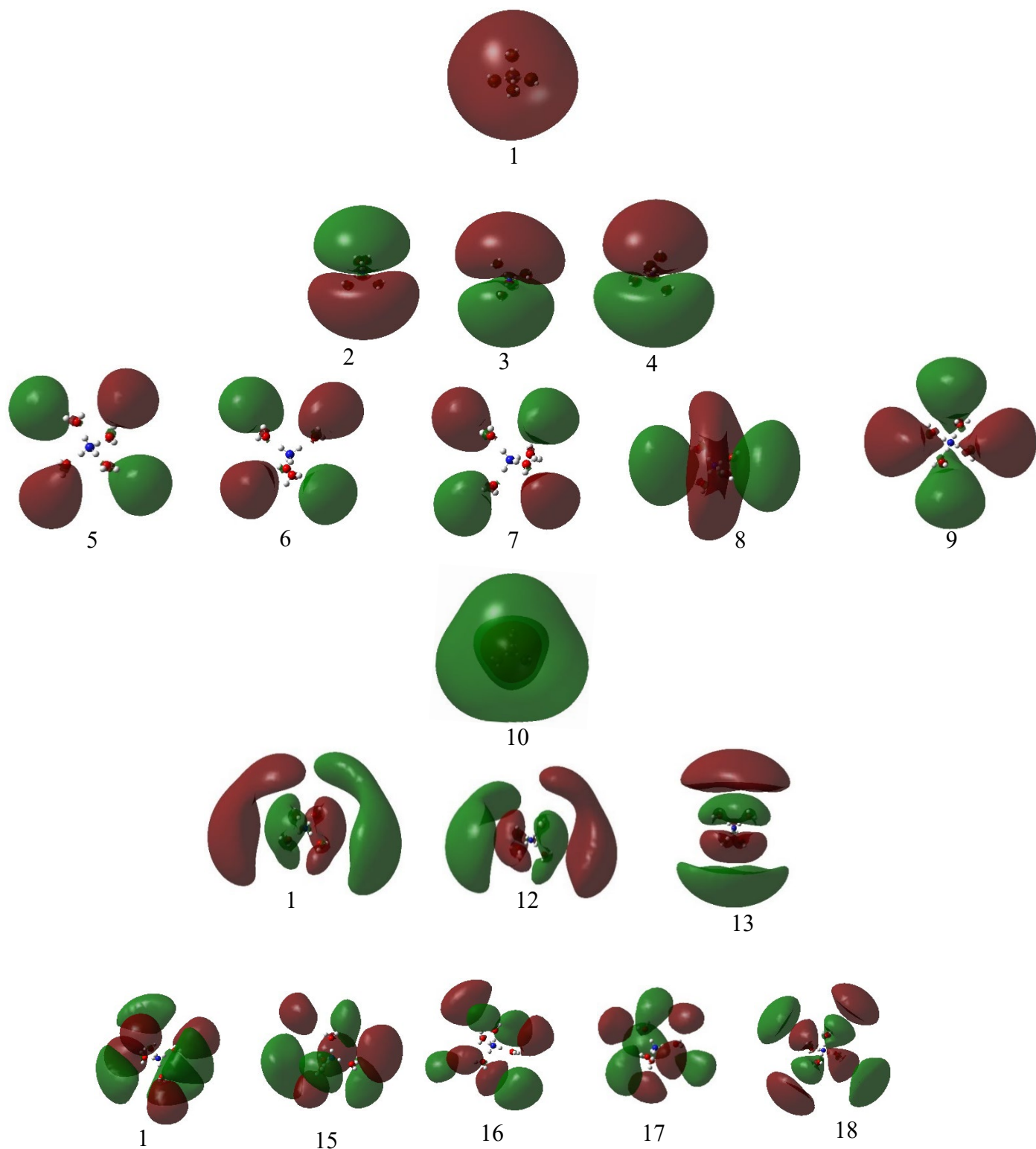


Figure 6: Dyson orbitals of electron attachment to the cation for ground and excited states of the tetrahedral $4e$ $\text{NH}_4(\text{H}_2\text{O})_4$ Rydberg radical. The numerical labels correspond to those in the second column of Table III (Dyson #).

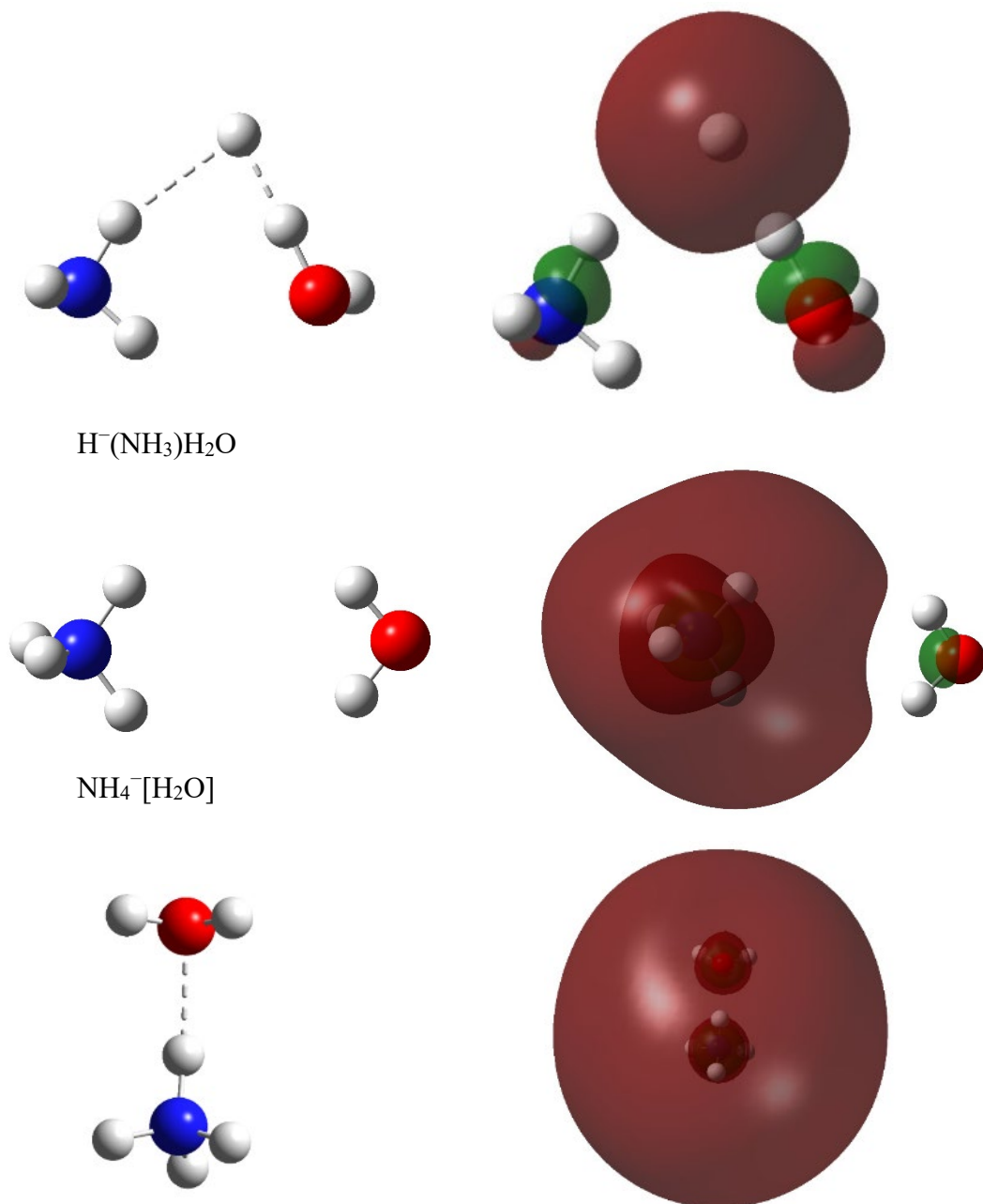


Figure 7: $n = 1$ Optimized geometries and Dyson orbitals of electron detachment from $\text{NH}_4^-(\text{H}_2\text{O})$ isomers.

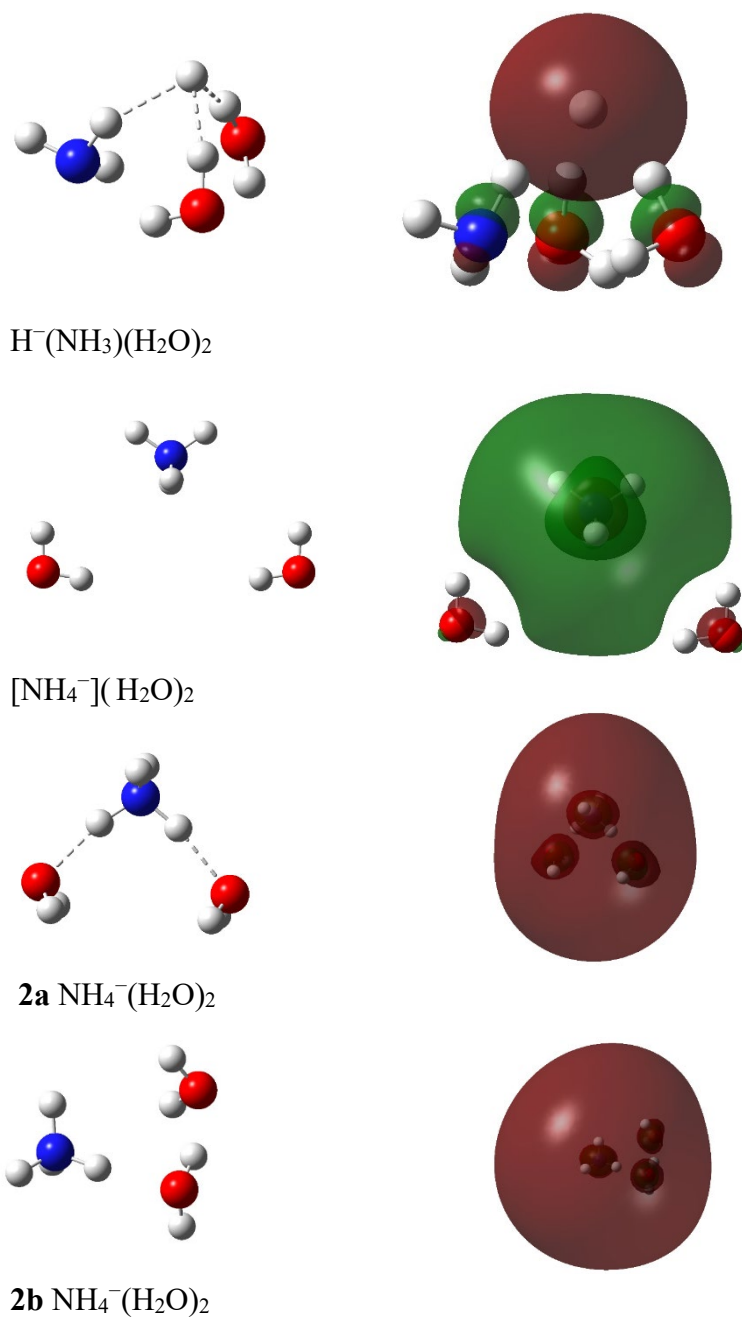


Figure 8: $n = 2$ Optimized geometries and Dyson orbitals of electron detachment from $\text{NH}_4^-(\text{H}_2\text{O})_2$ isomers.

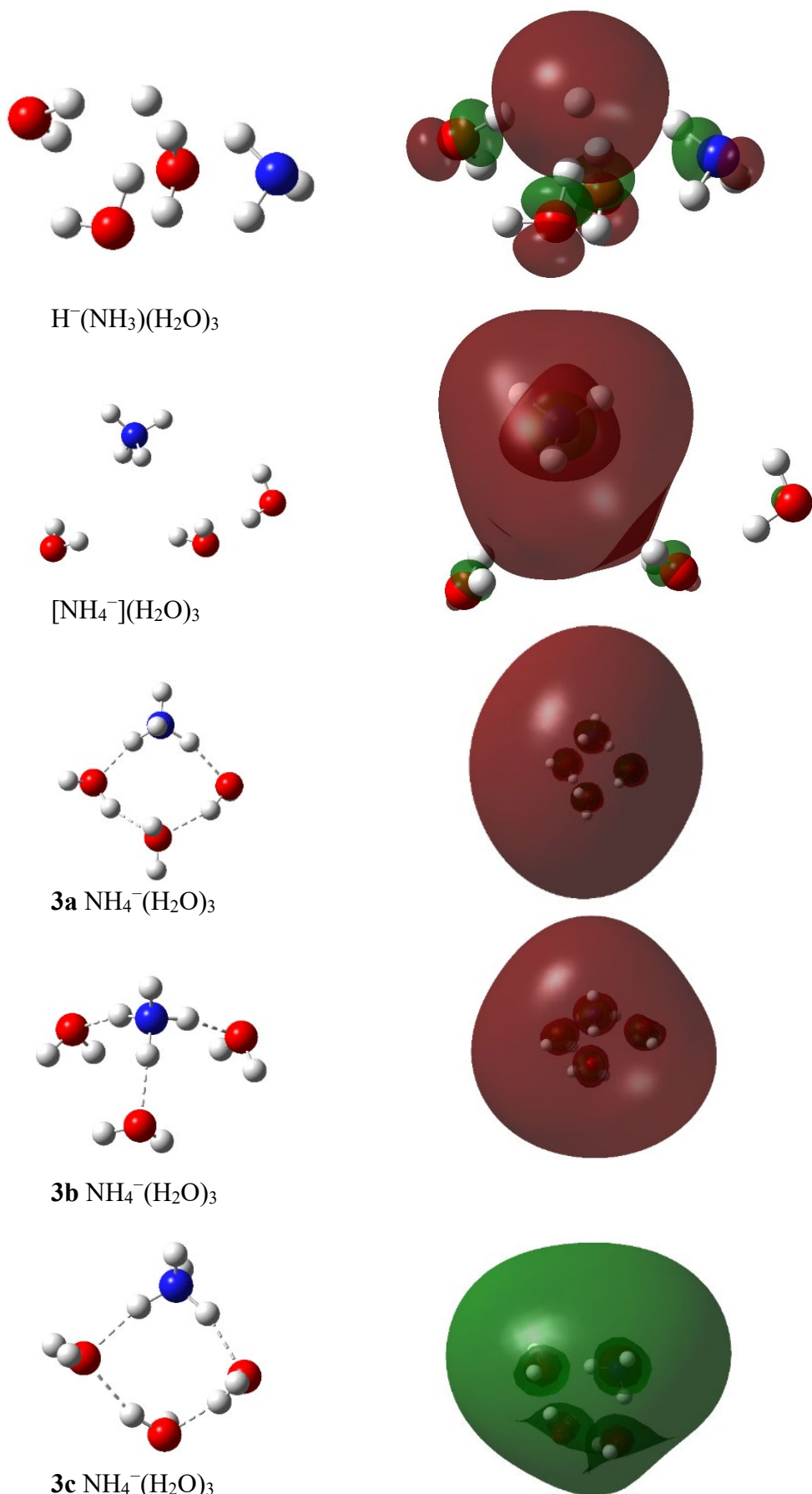


Figure 9: $n = 3$ Optimized geometries and Dyson orbitals of electron detachment from $\text{NH}_4^-(\text{H}_2\text{O})_3$ isomers.

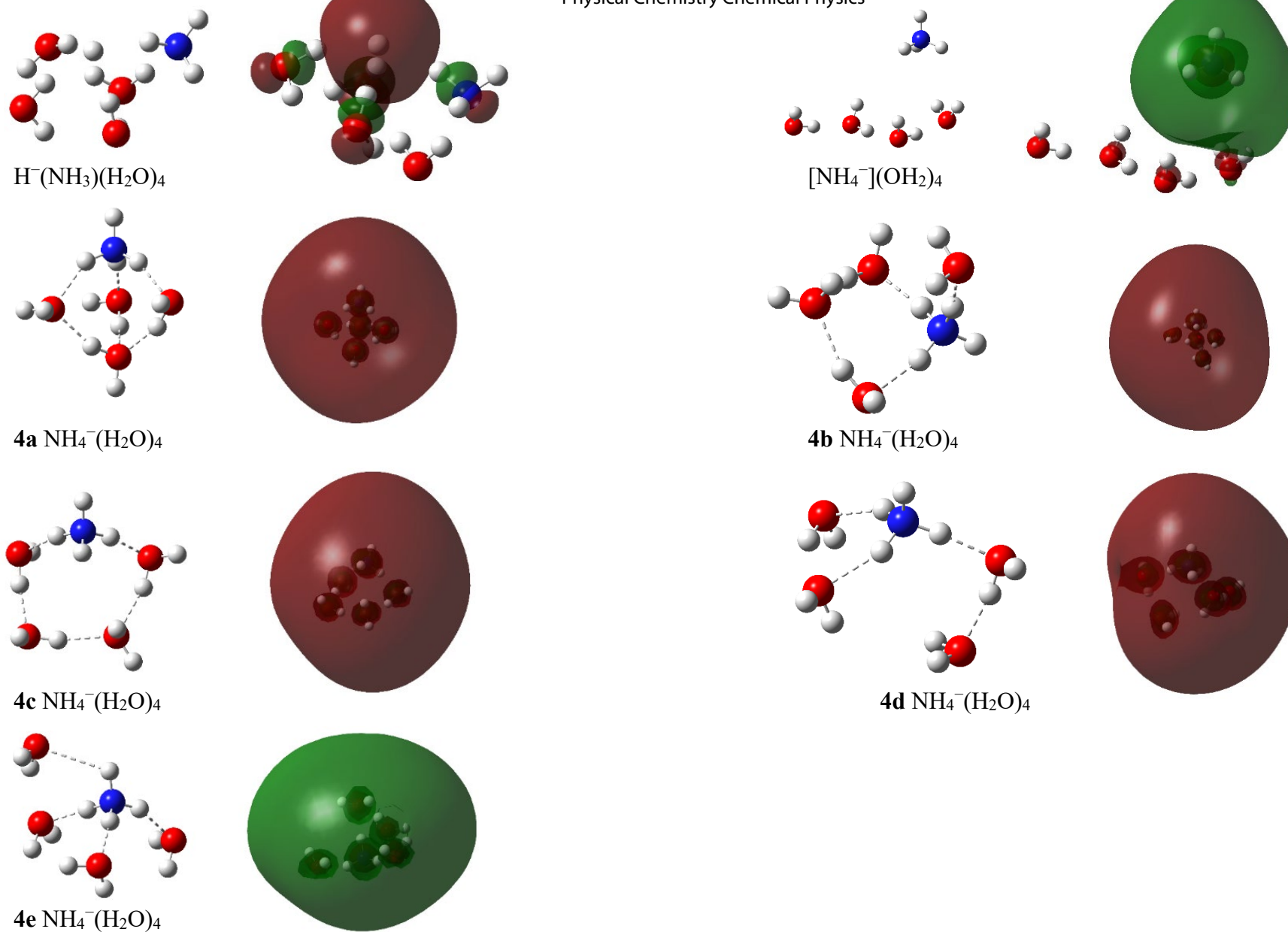


Figure 10: $n = 4$ Optimized geometries and Dyson orbitals of electron detachment from $\text{NH}_4^-(\text{H}_2\text{O})_4$ isomers.